Ketcham and Moonen
*J Wireless Com Network* (2025) 2025:11
https://doi.org/10.1186/s13638-025-02427-2

EURASIP Journal on Wireless Communications and Networking

RESEARCH Open Access

# Nonlinear power harvesting through $\alpha$-fair resource allocation in SWIPT

Richard Ketcham[1*] and Marc Moonen[1]

*Correspondence:
rich.ketcham@gmail.com

[1] STADIUS, KU Leuven, Department of Electrical Engineering (ESAT), Kasteelpark Arenberg 10 postbus 2440, Leuven 3001, Belgium

**Abstract**

The concurrent nature of multiuser (MU) simultaneous wireless information and power transfer (SWIPT), coupled with the complexity of orthogonal frequency division multiplexing (OFDM) and precoding, poses a challenging non-convex resource allocation problem. While conventional methods like subcarrier assignment or interference suppression can enhance tractability, they are not always optimal. Recent work has proposed leveraging hidden convexity in multicarrier systems to bypass these suboptimal methods, instead utilizing a multiple access channel (MAC)-broadcast channel (BC) duality for a near-optimal linear precoder design. However, this novel strategy relies on a linear power harvesting model, disregarding the nonlinear character of power harvesting in SWIPT networks. This paper addresses this issue by incorporating nonlinear power harvesting effects through a power harvesting model based on sigmoidal-like functions. Sigmoidal-like functions, being neither convex nor concave, typically necessitate transformation for tractability, a challenge compounded by the MAC-BC duality. We propose an alternate approach in which a parameterized class of utility functions known as $\alpha$-fairness is used to generalize the SWIPT resource allocation problem and concavify the nonlinear power harvesting model. This methodology simplifies optimization and facilitates the integration of nonlinear effects across a broad spectrum of fairness values.

**Keywords:** Energy harvesting, Fairness, Multiuser, Multicarrier, Multiantenna, Nonlinear, OFDM, Power harvesting, Resource allocation, Sigmoidal, SWIPT, Time-switching, Time-sharing

## 1 Introduction

The utility of an energy-constrained wireless network is often limited due to the reliance on finite energy resources. Owing to its potential to assuage this type of constraint, a technology termed simultaneous wireless information and power transfer (SWIPT) has garnered attention. By combining wireless communication and wireless power transfer concepts, SWIPT uses shared resources to deliver power and information simultaneously to remote wireless users thereby alleviating the limitations imposed by the energy constraints. SWIPT related research has covered a wide variety of topics since it was first introduced in [1–3], but primarily seeks to advance

Springer Open

© The Author(s) 2025. **Open Access** This article is licensed under a Creative Commons Attribution-NonCommercial-NoDerivatives 4.0 International License, which permits any non-commercial use, sharing, distribution and reproduction in any medium or format, as long as you give appropriate credit to the original author(s) and the source, provide a link to the Creative Commons licence, and indicate if you modified the licensed material. You do not have permission under this licence to share adapted material derived from this article or parts of it. The images or other third party material in this article are included in the article's Creative Commons licence, unless indicated otherwise in a credit line to the material. If material is not included in the article's Creative Commons licence and your intended use is not permitted by statutory regulation or exceeds the permitted use, you will need to obtain permission directly from the copyright holder. To view a copy of this licence, visit http://creativecommons.org/licenses/by-nc-nd/4.0/.

the utilization of limited system resources. Optimal resource allocation is crucial to improving the feasibility of SWIPT, so designing efficient resource allocation methods while incorporating technologies that improve power utilization, such as orthogonal frequency division multiplexing (OFDM) and precoding [4], is essential.

Multiuser (MU) SWIPT's concurrent nature, coupled with the complexity of OFDM and precoding, poses challenging non-convex resource allocation problems. While mitigating user interference through orthogonal frequency division multiple access (OFDMA) or zero forcing (ZF) precoding is a common way to enhance tractability, they are optimal only under high interference conditions [5, 6]. In contrast, a novel method in [7] exploits hidden convexity in multicarrier systems [8, 9] to solve non-convex problems via Lagrangian decomposition, bypassing OFDMA and ZF precoding. This approach leverages a multiple access channel (MAC)-broadcast channel (BC) duality to simplify precoder design, linking the problem to the dual MAC symbol power. However, this duality treats user interference as noise linearly related to the precoding vectors, necessitating the use of a linear power harvesting model over nonlinear alternatives. In this paper, we seek to include nonlinear power harvesting effects in the resource allocation method developed in [7].

Unlike traditional wireless communication networks, a SWIPT network must contend with power harvesting where received radio frequency (RF) power is converted to direct current (DC) power via a rectifier. Hence, incorporating an accurate power harvesting model is a critical aspect of resource allocation for SWIPT. It is well known that power harvesting is nonlinear [10]. Yet, many works utilize a linear harvesting model for tractability [11, 12], with some citing an ability to place several power harvesting circuits in parallel to enlarge the linear power conversion region as justification [7]. Two means for considering nonlinear effects include the diode nonlinear model and the saturation nonlinear model [10]. The diode nonlinear model is based on the physics of the specific circuit while the saturation nonlinear model is based on curve fitting to circuit measurements.

The diode nonlinear model is useful for setting phases and amplitudes required in waveform design. It is based on the small-signal model around an induced quiescent point, operating in the transition region between the square law region and the linear region [13]. However, as the RF input power increases, the harvesting circuit enters the linear region and eventually saturates causing the small-signal model to no longer hold [14]. In contrast, the saturation nonlinear model is a tractable method for modeling the linear and saturation regions of the harvesting circuitry. While it may have mild discrepancies in the low-power region [10], from a power allocation perspective it is arguably more important to avoid entering saturation. As such, the saturation nonlinear model is more applicable to improving the power allocation method designed in [7].

A practical saturation nonlinear harvesting model for SWIPT using a sigmoidal-like function was first proposed in [15] and has since become widely adopted [16–18]. A function $f(x)$ is sigmoidal-like if it has one inflection point $x_0$, with negative curvature for $x > x_0$ and positive curvature for $x < x_0$ [19]. Due to this changing curvature, the model proposed in [15] is neither convex nor concave [20], so directly incorporating it into an optimization problem requires additional methods to solve [15, 16]. The authors in [21]

also used a sigmoidal-like utility function for bandwidth allocation in a 4G cellular network. Interestingly, [21] showed that a sigmoidal-like function encapsulated with only a proportionally fair (logarithmic) utility function is strictly concave.

Noting that a logarithmic utility function limits the range of fairness to only proportionally fair, we first seek to expand on the results in [21] by generalizing to a parameterized class of utility functions collectively referred to as $\alpha$-fairness. These utilities allow for the specification of a relative degree of fairness, ranging from weighted fairness to maximizing the minimum (i.e. max-min) amount of fairness. Next, we solve for the minimum amount of fairness required to make the resulting $\alpha$-fair sigmoidal-like function (referred to as a composite utility) strictly concave. The concavity of the composite utility simplifies incorporating nonlinear harvesting effects into the SWIPT resource allocation compared to [15]. Lastly, despite being concave, it is a challenge to apply the MAC-BC duality to the composite utility. A method is developed to apply the composite utility to the SWIPT resource allocation presented in [7], enabling it to easily incorporate nonlinear harvesting effects for a large range of fairness values.

*Contributions:*

This paper first extends the novel algorithm presented in [7] by

- allocating resources relatively based on weights instead of specific harvesting constraints,
- generalizing the resource allocation by incorporating fairness between the objectives through $\alpha$-fairness utility functions,
- and by replacing the linear power harvesting model with a nonlinear power harvesting model.

With regard to the nonlinear power harvesting model, the paper makes the following contributions:

- [21] showed that a sigmoidal-like function encapsulated by a log function (for proportional fairness) is strictly concave. This result is extended by showing that encapsulating the sigmoidal-like function in the $\alpha$-fairness utility functions results in a composite function that is strictly concave for fairness values greater than a certain value ($\beta_{\text{MIN}}$), which is a much larger range of fairness values than the single value studied in [21].
- This paper provides an equation for $\beta_{\text{MIN}}$ based on the power harvester model parameters.
- Through $\alpha$-fairness, the sigmoidal-like function can be incorporated as-is without requiring an additional problem transformation and the associated iteration described in [15].

*Notation:* Matrices are upright and sans-serif, vectors are italicized and bold, and scalars are italicized. Sets are upright, serif, and italicized. The transpose operation is denoted with $(\cdot)^\top$, Hermitian transpose is $(\cdot)^{\mathcal{H}}$, and $\mathbb{E}[\cdot]$ is the expected value operator. The $\mathit{diag}(\cdot)$ operator returns a diagonal matrix with the diagonal elements given by its argument. A set is denoted with $\{\cdot_i\}_{\forall i}$, where $i$ is an index and $\cdot_i$ is the $i$-th object in the set. The Hadamard product is given by $\circ$.

## 2 Methods

### 2.1 Network

Consider the SWIPT network illustrated in Fig. 1, which contains one access point and $N$ remote devices (users), each with one antenna. Wireless transmissions are modeled as a multiple-input single-output (MISO) BC in which the access point uses $N_T$ transmit antennas to deliver data and power to the $N$ users, where $N \leq N_T$. The $N \leq N_T$ constraint enables the network to employ full multiuser interference suppression when the conditions are appropriate. The network employs OFDM, where the OFDM symbols are comprised of $K$ orthogonal subcarriers. It is assumed that perfect channel state information (i.e., the channel measurements are complete and accurate) is available and each subcarrier may be modeled independently due to the absence of inter-carrier interference.

### 2.2 Broadcast channel

The access point applies a precoder to the symbol vector before transmitting to the users, which is modeled on each subcarrier (denoted with subscript $k$) as a BC with

$$\boldsymbol{y}_k = \mathsf{H}_k^{\mathcal{H}} \mathsf{T}_k \boldsymbol{x}_k + \boldsymbol{z}_k. \tag{1}$$

In (1), $\boldsymbol{y}_k$ is the $N \times 1$ complex vector of symbols as received by the $N$ users, ${\mathsf{H}_k}^{\mathcal{H}}$ is the $N \times N_T$ complex channel matrix, with $[\mathsf{H}_k]_{m,n}^{\mathcal{H}}$ being the channel matrix between transmit antenna $m$ and user $n$ evaluated at subcarrier $k$, $\mathsf{T}_k$ is the $N_T \times N$ linear complex precoder matrix, $\boldsymbol{x}_k$ is the $N \times 1$ vector of complex transmit symbols for the $N$ users, and $\boldsymbol{z}_k$ is an $N \times 1$ complex vector of circularly symmetric additive white Gaussian noise (AWGN) where the distribution of the $n$-th element is denoted as $z_{k,n} \sim \mathcal{CN}(0, \sigma_{k,n})$ with zero mean and variance $\sigma_{k,n}$.

The received signal at user $n$ on subcarrier $k$ is the $n$-th row of (1) and is modeled with

$$y_{k,n} = \boldsymbol{h}_{k,n}^{\mathcal{H}} \boldsymbol{t}_{k,n} x_{k,n} + \sum_{\substack{m=1 \\ m \neq n}}^{N} \boldsymbol{h}_{k,n}^{\mathcal{H}} \boldsymbol{t}_{k,m} x_{k,m} + z_{k,n}, \tag{2}$$

where $\boldsymbol{t}_{k,n}$ is the precoder vector for user $n$, i.e., the $n$-th column of $\mathsf{T}_k$, $\boldsymbol{h}_{k,n}$ is the channel vector for user $n$, i.e., the $n$-th column of $\mathsf{H}_k$, and $x_{k,n}$ is the $n$-th element of $\boldsymbol{x}_k$. The first term, given by $\boldsymbol{h}_{k,n}^{\mathcal{H}} \boldsymbol{t}_{k,n} x_{k,n}$, is the signal intended for user $n$. The second term, given by $\sum_{\substack{m=1 \\ m \neq n}}^{N} \boldsymbol{h}_{k,n}^{\mathcal{H}} \boldsymbol{t}_{k,m} x_{k,m}$, is the interference from the signals intended for the other users.

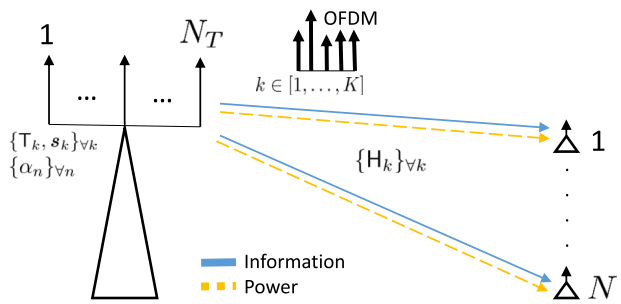


**Fig. 1** OFDM-based MU-MISO-BC-SWIPT system diagram

### 2.3 Metrics

The downstream data rate for user $n$ on subcarrier $k$ is modeled with

$$R_{k,n}(\mathsf{T}_k, \boldsymbol{s}_k) = \log_2\left(1 + \gamma_{k,n}^{\mathrm{BC}}(\mathsf{T}_k, \boldsymbol{s}_k)\right) \tag{3}$$

and the total data rate for user $n$, $rd_n$, is calculated by summing (3) over all subcarriers

$$rd_n = \sum_{k=1}^{K} R_{k,n}(\mathsf{T}_k, \boldsymbol{s}_k). \tag{4}$$

The downstream signal-to-interference-plus-noise ratio (SINR) for user $n$ on subcarrier $k$, $\gamma_{k,n}^{\mathrm{BC}}(\mathsf{T}_k, \boldsymbol{s}_k)$, is a function of the precoder matrix $\mathsf{T}_k$ and symbol power vector $\boldsymbol{s}_k$. The $n$ -th element of $\boldsymbol{s}_k$, denoted by $s_{k,n}$, is the real-valued symbol power for user $n$. It is defined as $s_{k,n} \triangleq \mathbb{E}\left[|x_{k,n}|^2\right]$, where $\mathbb{E}[\cdot]$ is the expected value operator. The SINR is given by

$$\gamma_{k,n}^{\mathrm{BC}}(\mathsf{T}_k, \boldsymbol{s}_k) = \frac{|\boldsymbol{t}_{k,n}^{\mathcal{H}} \boldsymbol{h}_{k,n}|^2 s_{k,n}}{\sum_{\substack{m=1 \\ m \neq n}}^{N} |\boldsymbol{t}_{k,m}^{\mathcal{H}} \boldsymbol{h}_{k,n}|^2 s_{k,m} + \sigma_{k,n}}, \tag{5}$$

where $\sigma_{k,n}$ is the AWGN power experienced by user $n$ on subcarrier $k$, $|\boldsymbol{t}_{k,n}^{\mathcal{H}} \boldsymbol{h}_{k,n}|^2 s_{k,n}$ is the received power of the signal intended for user $n$, and $\sum_{\substack{m=1 \\ m \neq n}}^{N} |\boldsymbol{t}_{k,m}^{\mathcal{H}} \boldsymbol{h}_{k,n}|^2 s_{k,m}$ is the interference power from the signals intended for the other users.

The received power for user $n$ on subcarrier $k$ is modeled with

$$P_{k,n}(\mathsf{T}_k, \boldsymbol{s}_k) = \sum_{m=1}^{N} |\boldsymbol{t}_{k,m}^{\mathcal{H}} \boldsymbol{h}_{k,n}|^2 s_{k,m}, \tag{6}$$

and the total received power for user $n$ ($rp_n$) is calculated by summing (6) over all subcarriers in

$$r_{p_n} = \sum_{k=1}^{K} P_{k,n}(\mathbf{T}_k, \mathbf{s}_k). \tag{7}$$

Similarly, the total transmit power $p_n$ for user $n$ is calculated by summing the transmit power over all subcarriers and may be modeled with

$$p_n = \sum_{k=1}^{K} s_{k,n} ||\boldsymbol{t}_{k,n}||_2^2. \tag{8}$$

### 2.4 Basics of power harvesting

Combining an antenna with a power[1] harvester creates a rectenna. The purpose of the rectenna is to convert RF power to DC power since most electronics in a wireless device require

[1] Note that the harvesting circuit is often referred to as an energy harvester, but since the duration of the time slot is not considered in this paper, it will be generally referred to as a power harvester.

a DC power source to operate. The rectenna operates by first converting an electromagnetic signal to an electrical signal via the antenna. The electrical signal is then rectified and filtered. The DC power may then be utilized to power specific circuits, charge a battery, or charge a supercapacitor.

A variety of diode technologies and topologies (e.g., half-wave, full-wave, voltage doubler, etc.) are utilized in rectennas [10]. Figure 2 illustrates the simplest rectenna, employing a half-wave topology consisting of an antenna, an impedance matching network, a diode, and a low-pass filter to reduce the voltage ripple. The diode plays an outsized role in the circuit because it remains non-conductive for voltages below its turn-on threshold and enters breakdown for voltages exceeding its breakdown voltage. When the diode reaches breakdown, the output power of the rectifier circuit saturates, leading to a decrease in power conversion efficiency. As a result, the power conversion efficiency is a nonlinear function of the RF input power, decreasing at higher input levels once the breakdown voltage is surpassed.

### 2.5 Harvested power model

While [7] modeled the harvested power as linearly proportional to (7) for tractability, the power harvesting operation is nonlinear in general [10]. A practical nonlinear harvesting model for SWIPT using a sigmoidal-like function was first proposed in [15]. Here, we use a normalized sigmoidal-like utility function [21] in place of [15], given as

$$U^{\sigma}(rp_n) = c\Big((1+\psi_n)^{-1} - d\Big), \tag{9}$$

where

$$\begin{aligned} \psi_n &= e^{-a(rp_n - b)}, \\ c &= \frac{1+e^{ab}}{e^{ab}}, \\ d &= \frac{1}{1+e^{ab}}, \end{aligned} \tag{10}$$

and $rp_n$ is the RF power present at the antenna for user $n$ as given in (7). Parameters $a$ and $b$ are positive and chosen experimentally, where $a$ represents the nonlinear charging rate (i.e., steepness of the curve) and $b$ represents the minimum turn-on power [10]. Consequently, $\psi_n > 0$, $c > 0$, and $d > 0$. The harvester parameters may differ between

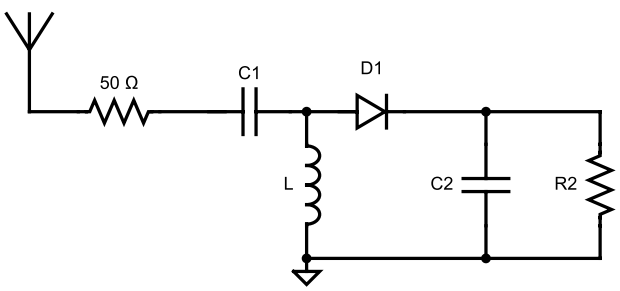


**Fig. 2** A half-wave rectenna circuit

users, but for the sake of clarity, they are assumed to be the same for all users without loss of generality (w.l.o.g).

The model satisfies $U^{\sigma}(0) = 0$ and $U^{\sigma}(\infty) = 1$. Scaling $U^{\sigma}$ with the harvester saturation power, $P_{\mathrm{SAT}}$, calculates the DC power produced by the harvester and is equivalent to the model proposed in [15]. The scaling with $P_{\mathrm{SAT}}$ is omitted here, as it is undone by the later normalization in (16) anyway. Example harvester settings are illustrated in Fig. 3. It is important to note that sigmoidal-like functions are non-convex and non-concave.

### 2.6 Time-switching

A time-switching SWIPT receiver is considered, which performs either information decoding or power harvesting [3] by using a high-speed RF switch to connect the antenna to either circuit. The duration for either action is determined by the time-switching ratio, given by $\alpha_n \in [0, 1]$ for user $n$, where the receiver for user $n$ spends $\alpha_n$ proportion of time decoding information and $1 - \alpha_n$ proportion of time harvesting power. Hence, the data rate for user $n$ due to time-switching is given by

$$\tilde{rd}_n = \alpha_n rd_n. \tag{11}$$

Similarly, the harvested power for user $n$ due to time-switching is given by

$$\tilde{r}_{p_n} = (1 - \alpha_n) U^{\sigma}(r_{p_n}). \tag{12}$$

The time-switching ratios will not be optimized, i.e., will be considered constant.

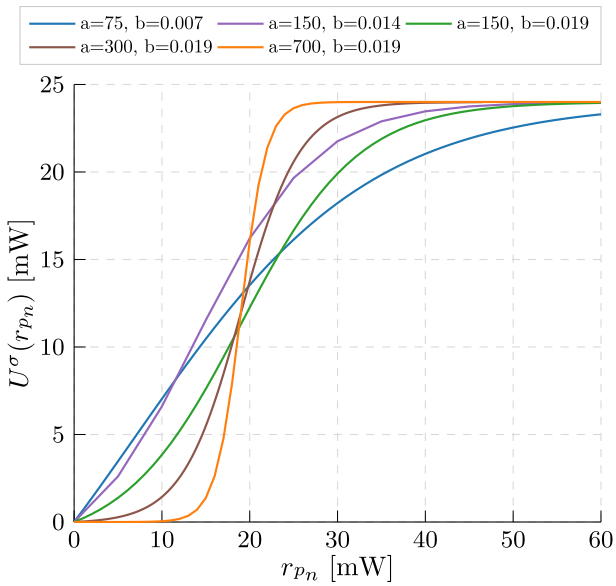


**Fig. 3** The sigmoidal-like nonlinear power harvester model is illustrated here for several sets of parameters with $P_{\mathrm{SAT}} = 24$ mW

## 3 Primal problem

In [7], the resource allocation problem was formulated as a weighted sum of data rates subject to meeting a total transmit power constraint and individual user power harvesting constraints. In this paper, the resource allocation is generalized to incorporate fairness between objectives rather than meeting specific power harvesting constraints as well as include the nonlinear effects of the power harvester. As noted, [7] utilized a MAC-BC duality that necessitated modeling the power harvesting efficiency as linear. For SWIPT receivers that cannot dynamically expand the linear harvesting region, modeling the harvester efficiency as linear is a significant problem because it ignores the dependence of the harvester efficiency on the input power. The problem is particularly acute when the power harvester saturates. If power is allocated beyond the point of saturation, the harvester efficiency decreases significantly and power allocated beyond this point is essentially wasted. Incorporating the nonlinear harvesting effects will allow the resource allocation to reallocate power toward improving the other objectives.

### 3.1 $\alpha$-Fair Utility Function

A generalized mathematical formulation for fair resource allocation called $\alpha$-fairness was proposed in [22]. $\alpha$-fairness describes a class of mostly nonlinear utility functions that promote varying degrees of fairness from weighted fairness to max-min fairness. The utility functions defined by $\alpha$-fairness utilize a parameter that is usually denoted with $\alpha$ but will be denoted with $\beta$ here to avoid confusion with the time-switching ratios. The utility functions are then defined as

$$f^{\beta}(\{z_n\}) = \begin{cases} \sum_{n=1}^{N} \mu_n \frac{(z_n)^{1-\beta}}{(1-\beta)}, & \beta \geq 0, \beta \neq 1 \\ \sum_{n=1}^{N} \mu_n \ln(z_n), & \beta = 1 \end{cases}, \tag{13}$$

where $\{z_n\}_{\forall n}$ represents the objectives, $\mu_n$ is a weight associated with the $n^{\text{th}}$ objective, and $\beta$ is the fairness parameter. As the fairness parameter $\beta$ increases, the resource allocation becomes increasingly fair in that the resulting objectives are increasingly equivalent. Note that the natural logarithm is used for $\beta = 1$ and when $\beta = 0$, (13) reduces to a linear utility function (i.e., weighted sum utility function).

### 3.2 Normalization

With $\alpha$-fairness, it is paramount to appropriately scale the objectives by the associated range of values otherwise there may be a bias. Assuming constant time-switching ratios, then the maximum power harvester utility is given by

$$U_{\text{MAX}}^{\sigma} = \max\left(\left\{\tilde{rp}_n^{\text{MAX}}\right\}_{\forall n}\right), \tag{14}$$

and the maximum data rate is given by

$$R_{\text{MAX}} = \max\left(\left\{\tilde{rd}_n^{\text{MAX}}\right\}_{\forall n}\right). \tag{15}$$

For user $n$, the maximum possible harvested power is given by $\tilde{rp}_n^{\text{MAX}}$ and the maximum possible time-switched data rate is $\tilde{rd}_n^{\text{MAX}}$. The normalized harvested power and the normalized data rate are then

$$\hat{rp}_n = \frac{\tilde{rp}_n}{U^{\sigma}_{\mathrm{MAX}}} \text{ and } \hat{rd}_n = \frac{\tilde{rd}_n}{R_{\mathrm{MAX}}}, \tag{16}$$

for user $n$, respectively.

### 3.3 Primal problem formulation

Applying $\alpha$-fairness results in the following composite utility function

$$\begin{aligned} &\beta \neq 1, \beta \geq 0: \\ &\qquad \hat{f}^{\beta} = \sum_{n=1}^{N} \left( \frac{\hat{\mu} p_n}{(\hat{rp}_n)^{\beta-1}} + \frac{\hat{\mu} d_n}{(\hat{rd}_n)^{\beta-1}} \right) (1-\beta)^{-1}, \\ &\beta = 1: \\ &\qquad \hat{f}^{\beta} = \sum_{n=1}^{N} \hat{\mu} p_n \ln(\hat{rp}_n) + \hat{\mu} d_n \ln(\hat{rd}_n). \end{aligned} \tag{17}$$

The harvested power and data rate weights for user $n$ are given by $\hat{\mu} p_n$ and $\hat{\mu} d_n$, respectively. The weights are non-negative real valued and reflect the priority of the particular user data rate and harvested power. Additionally, the weights may be denoted in vector form where an $N \times 1$ vector of harvested power weights is denoted with $\hat{\boldsymbol{\mu}} p$ and an $N \times 1$ vector of data rate weights is denoted with $\hat{\boldsymbol{\mu}} d$. The basic problem formulation for the resource allocation is then given by

$$\begin{aligned} &\underset{\{\mathsf{T}_k, \boldsymbol{s}_k\}_{\forall k}}{\text{maximize}} \; \hat{f}^{\beta} \\ &\qquad \text{s.t.} \sum_{n=1}^{N} p_n \leq P_{\mathrm{Total}}, \\ &\qquad\quad s_{k,n} \geq 0 \quad \forall\, k, n \end{aligned} \tag{18}$$

where the total transmit power is constrained to be less than or equal to $P_{\mathrm{Total}}$. Note that if $\alpha_n \in \{0, 1\}$ either the harvested power objective or the data rate objective for user $n$ will need to be removed from the optimization because it will be unbounded from above otherwise. This can be done by setting $\hat{\mu} p_n = 0$ if $\alpha_n = 1$ or $\hat{\mu} d_n = 0$ if $\alpha_n = 0$.

Problem (18) is a non-convex optimization problem due to the design parameters. Yet, provided that the utility function $\hat{f}^{\beta}$ is non-decreasing and concave, it was shown that (18) enjoys a near-zero duality gap that vanishes asymptotically as the number of subcarriers goes to $\infty$ [9]. This facet is accomplished by interleaving resource allocations on a per-subcarrier basis and is known as the time-sharing property of multicarrier systems. As the number of subcarriers increase for a given total bandwidth, the width of each subcarrier becomes smaller leading to adjacent subcarriers experiencing similar fading characteristics that are increasingly flat and causing the duality gap to decrease. This paper considers OFDM, a multicarrier system that employs a guard interval known as a cyclic prefix. The cyclic prefix mitigates the effect of multipath which is responsible for frequency-selective fading. This means that an OFDM system with a practical number of subcarriers (e.g., $K = 64$) also enjoys a near-zero duality gap because adjacent subcarriers experience similar flat fading characteristics.

The objective $\hat{f}^{\beta}$ is indeed shown to be strictly concave with respect to (w.r.t.) $\{rp_n, rd_n\}_{\forall n}$ in Proposition 1, provided that the fairness parameter $\beta$ is greater than a minimum value $\beta_{\text{MIN}}$. Lemma 1 and Lemma 2 will provide the preliminaries for Proposition 1.

**Lemma 1** *The gradient of $\hat{f}^{\beta}$, $\nabla\hat{f}^{\beta}$, w.r.t. the resource allocation $\{rp_n, rd_n\}_{\forall n}$ is comprised of the partial derivatives given as*

$$\begin{aligned}\frac{\partial \hat{f}^{\beta}}{\partial rp_n} &= \frac{\hat{\mu} p_n}{(\hat{r}p_n)^{\beta}} \cdot \frac{1-\alpha_n}{U^{\sigma}_{\text{MAX}}} \cdot \frac{ca\psi_n}{(1+\psi_n)^2}, \\ \frac{\partial \hat{f}^{\beta}}{\partial rd_n} &= \frac{\hat{\mu} d_n}{(\hat{r}d_n)^{\beta}} \cdot \frac{\alpha_n}{R_{\text{MAX}}}\end{aligned} \tag{19}$$

*for all n and for $\beta \geq 0$. In addition, $\hat{f}^{\beta}$ is non-decreasing.*

***Proof*** The partial derivative of $\psi_n$, defined in (10), is

$$\frac{\partial}{\partial rp_n}\psi_n = -a\psi_n, \tag{20}$$

so the partial derivative of $U^{\sigma}(rp_n)$ defined in (9), is

$$\frac{\partial}{\partial rp_n}U^{\sigma}(rp_n) = \frac{ca\psi_n}{(1+\psi_n)^2}. \tag{21}$$

For $\beta \geq 0$ and $\beta \neq 1$, the partial derivatives of $\hat{f}^{\beta}$ w.r.t. $rp_n$ and $rd_n$ are

$$\begin{aligned}\frac{\partial}{\partial rp_n}\hat{f}^{\beta} &= \frac{\partial}{\partial \hat{r}p_n}\hat{f}^{\beta} \cdot \frac{\partial}{\partial rp_n}\hat{r}p_n \\ &= \frac{\hat{\mu} p_n}{(\hat{r}p_n)^{\beta}} \cdot \frac{1-\alpha_n}{U^{\sigma}_{\text{MAX}}} \cdot \frac{ca\psi_n}{(1+\psi_n)^2}, \\ \frac{\partial}{\partial rd_n}\hat{f}^{\beta} &= \frac{\hat{\mu} d_n}{(\hat{r}d_n)^{\beta}} \cdot \frac{\alpha_n}{R_{\text{MAX}}}.\end{aligned} \tag{22}$$

The utility function for $\beta = 1$ is given in (17), the partial derivatives of which results in the same expressions given in (22). Note that the partial derivatives are all non-negative, meaning that $\hat{f}^{\beta}$ is a non-decreasing function.

**Lemma 2** *The Hessian of $\hat{f}^{\beta}$, $\nabla^2\hat{f}^{\beta}$, w.r.t. the resource allocation $\{rp_n, rd_n\}_{\forall n}$ is a diagonal matrix, with the diagonal entries given in (26) and (27).*

***Proof*** The partial derivative w.r.t. $rp_n$ in (22) can be put in terms of $\psi_n$ using the definition of $U^{\sigma}(rp_n)$ in (9)

$$\begin{aligned}\frac{\partial}{\partial rp_n}\hat{f}^{\beta} &= \frac{\hat{\mu}p_n}{(\hat{r}p_n)^{\beta}} \cdot \frac{1-\alpha_n}{U^{\sigma}_{\mathrm{MAX}}} \cdot \frac{ca\psi_n}{(1+\psi_n)^2} \\ &= \frac{\hat{\mu}p_n}{\left(\frac{(1-\alpha_n)c}{U^{\sigma}_{\mathrm{MAX}}}((1-\psi_n)^{-1}-d)\right)^{\beta}} \cdot \frac{ca\psi_n(1-\alpha_n)}{U^{\sigma}_{\mathrm{MAX}}(1+\psi_n)^2} \\ &= \frac{\hat{\mu}p_n a}{\left(\frac{(1-\alpha_n)c}{U^{\sigma}_{\mathrm{MAX}}}\right)^{\beta-1}} \cdot \frac{(1+\psi_n)^{\beta-2}\psi_n}{(1-d(1+\psi_n))^{\beta}}.\end{aligned} \tag{23}$$

Let

$$\begin{aligned}A &= (1+\psi_n)^{\beta-2}\psi_n, \\ B &= (1-d(1+\psi_n))^{-\beta},\end{aligned} \tag{24}$$

then

$$\begin{aligned}\frac{\partial}{\partial rp_n}A &= -a\psi_n\Big((1+\psi_n)^{\beta-2} + \psi_n(\beta-2)(1+\psi_n)^{\beta-3}\Big), \\ \frac{\partial}{\partial rp_n}B &= -a\psi_n\Big(d\beta(1-d(1+\psi_n))^{-\beta-1}\Big).\end{aligned} \tag{25}$$

Through the product rule, the second partial derivative w.r.t. $rp_n$ is given by

$$\begin{aligned}\frac{\partial^2}{\partial rp_n \partial rp_n}\hat{f}^{\beta} &= \frac{\hat{\mu}p_n a}{\left(\frac{(1-\alpha_n)c}{U^{\sigma}_{\mathrm{MAX}}}\right)^{\beta-1}}\left(\frac{\partial A}{\partial rp_n}B + \frac{\partial B}{\partial rp_n}A\right) \\ &= \frac{-\hat{\mu}p_n a^2\psi_n(1+\psi_n)^{\beta-2}}{\left(\frac{(1-\alpha_n)c}{U^{\sigma}_{\mathrm{MAX}}}\right)^{\beta-1}}\left[\frac{d\beta\psi_n}{(1-d(1+\psi_n))^{\beta+1}}\right. \\ &\quad \left. + \frac{1}{(1-d(1+\psi_n))^{\beta}} + \frac{(\beta-2)\psi_n}{(1+\psi_n)(1-d(1+\psi_n))^{\beta}}\right].\end{aligned} \tag{26}$$

The second partial derivative w.r.t. $rd_n$ is

$$\frac{\partial^2}{\partial rd_n \partial rd_n}\hat{f}^{\beta} = \frac{-\beta\hat{\mu}d_n}{(\hat{r}d_n)^{\beta+1}}\left(\frac{\alpha_n}{R_{\mathrm{MAX}}}\right)^2. \tag{27}$$

Lastly, observe that the partial derivatives w.r.t. $rp$ do not depend on $rd$ and vice versa, nor do the partial derivatives for user $n$ depend on user $j$ for $n \neq j$. Hence,

$$\begin{aligned}\frac{\partial^2}{\partial rp_n \partial rp_j}\hat{f}^{\beta} &= 0 \;\forall\; n \neq j, \\ \frac{\partial^2}{\partial rd_n \partial rd_j}\hat{f}^{\beta} &= 0 \;\forall\; n \neq j, \\ \frac{\partial^2}{\partial rp_n \partial rd_j}\hat{f}^{\beta} &= 0 \;\forall n, j \in [1, N].\end{aligned} \tag{28}$$

Since all terms are 0 except for those on the main diagonal, the Hessian is a diagonal matrix.

**Proposition 1** *The composite utility function described in* (17) *is strictly concave w.r.t.* $\{rp_n, rd_n\}\forall n$ *for* $\beta > \beta_{\text{MIN}} = 1 - \frac{2\sqrt{e^{ab}}}{1+e^{ab}}$.

***Proof*** The received RF power for user $n$, $rp_n$, is non-negative. For non-negative values, the sigmoidal-like utility function can be bounded [21] with

$$\begin{aligned} &0 \leq U^{\sigma}(rp_n) \leq 1, \\ &0 \leq c((1+\psi_n)^{-1} - d) \leq 1, \\ &d \leq (1+\psi_n)^{-1} \leq \frac{1+cd}{c}. \end{aligned} \tag{29}$$

Inverting and rearranging, we arrive at

$$\begin{aligned} &\frac{1}{d} \geq (1+\psi_n) \geq \frac{c}{1+cd}, \\ &0 \geq d(1+\psi_n) - 1 \geq \frac{cd}{1+cd} - \frac{1+cd}{1+cd}, \\ &0 \leq 1 - d(1+\psi_n) \leq \frac{1}{1+cd}. \end{aligned} \tag{30}$$

Lemma 2 showed that $\nabla^2 \hat{f}^{\beta}$ is a diagonal matrix, so it is strictly concave when all of the diagonal entries, defined by (26) and (27), are negative. The diagonal entries described in (27) are negative for all $\beta > 0$. The diagonal entries described in (26) are negative if

$$\frac{d\beta\psi_n}{(1-d(1+\psi_n))^{\beta+1}} + \frac{1}{(1-d(1+\psi_n))^{\beta}} + \frac{(\beta-2)\psi_n}{(1+\psi_n)(1-d(1+\psi_n))^{\beta}} > 0. \tag{31}$$

Note that since $d > 0$, $\psi_n > 0$, and $(1 - d(1+\psi)) \geq 0$ from (30), it is immediately clear that (26) is negative for $\beta \geq 2$. Finding the common denominator of (31) and multiplying through, we arrive at

$$(\beta-2)\psi_n(1-d(1+\psi_n)) + (1+\psi_n)(1-d(1+\psi_n)) + d\beta\psi_n(1+\psi_n) > 0. \tag{32}$$

Solving for $\beta$, we arrive at

$$\beta > (1-\psi_n^{-1})(1-d(1+\psi_n)) = g(rp_n). \tag{33}$$

Thus, $\hat{f}^{\beta}$ is strictly concave as long as $\beta$ is greater than $g(rp_n)$ for all values of $rp_n \geq 0$, i.e.,

$$\beta > \max_{rp_n \geq 0} g(rp_n). \tag{34}$$

Let us solve for the value of $rp_n$ that yields the largest lower bound $\beta_{\text{MIN}}$ for $\beta$. Distributing terms

$$\begin{aligned} g(rp_n) &= (1-\psi_n^{-1})(1-d(1+\psi_n)) \\ &= (1-\psi_n^{-1}) - d(\psi_n - \psi_n^{-1}) \\ &= 1 - \psi_n^{-1}(1-d) - d\psi_n, \end{aligned} \tag{35}$$

$g(rp_n)$ can be shown to be concave by first taking the first derivative

$$\begin{aligned}\frac{\partial}{\partial rp_n} g(rp_n) &= \frac{\partial}{\partial \psi_n} g(rp_n) \frac{\partial}{\partial rp_n} \psi_n \\ &= (\psi^{n^{-2}}(1-d) - d)(-a\psi_n) \\ &= ad\psi_n - a\psi_n^{-1}(1-d),\end{aligned} \tag{36}$$

and then the second derivative

$$\frac{\partial^2}{\partial {rp_n}^2} g(rp_n) = -(a^2\psi_n^{-1}(1-d) + a^2 d\psi_n) < 0. \tag{37}$$

Since $a$ is positive and real, $\psi > 0$, and $(1-d) > 0$, the second derivative is negative and is thus strictly concave. Hence, we can solve for the unique value of $rp_n$ that yields the largest $g(rp_n)$ by setting the first derivative (36) to 0, i.e.,

$$\begin{aligned} ad\psi_n - a\psi_n^{-1}(1-d) &= 0, \\ \psi_n^2 &= \frac{1-d}{d}, \\ \psi_n &= \sqrt{1 + e^{ab} - 1}, \\ e^{-arp_n} e^{ab} &= \sqrt{e^{ab}}, \\ rp_n &= \frac{\ln(\sqrt{e^{-ab}})}{-a}. \end{aligned} \tag{38}$$

Note that $0 < \sqrt{e^{-ab}} < 1$, so $\ln(\sqrt{e^{-ab}}) < 0$ and $rp_n > 0$. Substituting (38) into (33), we arrive at the following bound $\beta_{\text{MIN}}$ for strict concavity

$$\begin{aligned}\beta_{\text{MIN}} =& g\left(\ln(\sqrt{e^{-ab}})(-a)^{-1}\right) \\ =& 1 - \sqrt{e^{ab}}^{-1}(1-d) - d\sqrt{e^{ab}} \\ =& 1 - \frac{2e^{ab}}{\sqrt{e^{ab}}(1+e^{ab})} \\ =& 1 - \frac{2\sqrt{e^{ab}}}{1+e^{ab}}.\end{aligned} \tag{39}$$

Figure 4 illustrates $g(rp_n)$. Setting $\beta > \beta_{\text{MIN}}$ will make $\hat{f}^\beta$ strictly concave for all values of $rp_n$. As (39) indicates, the bound is not dependent on $rp_n$, but on the harvester parameters. Provided that all users have the same harvester parameters, then all users will have the same $\beta_{\text{MIN}}$. Figure 5 illustrates that the α-fair utility is non-concave for $\beta < \beta_{\text{MIN}}$. Conversely, Fig. 6 illustrates that the α-fair utility is concave for $\beta > \beta_{\text{MIN}}$. Note that each trace in Fig. 5 is scaled by $\max |f^\beta(U^\sigma(rp_n))|$ to better compare the curvatures. The traces in Fig. 6 are not scaled since they have similar magnitudes and it is easy to see that they are concave.

### 3.4 Linearization

Since $\hat{f}^\beta$ is strictly concave for an appropriate $\beta$ and the domain is convex due to time-sharing [9, 20], (18) can be solved through the conditional gradient method [23] by linearizing (17) and maximizing iteratively. The partial derivative of (17) is given in Lemma 1. The linearized objective is then expressed as

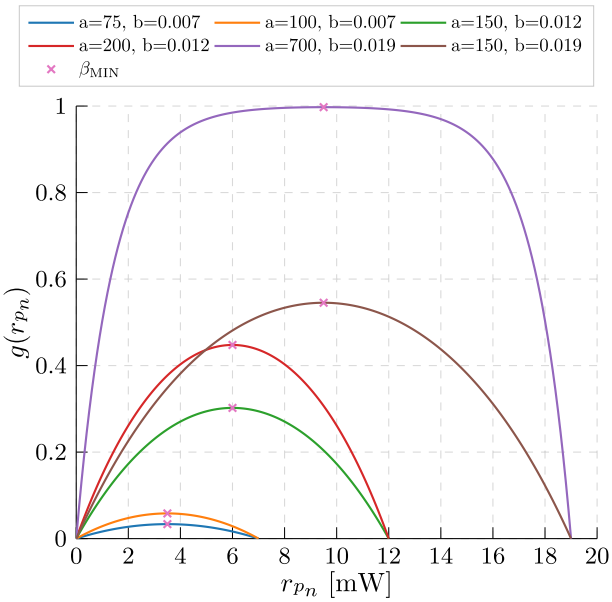


**Fig. 4** $g(rp_n)$ as a function of $rp_n$ and various model parameters. $\beta_{\text{MIN}}$ is the maximum value

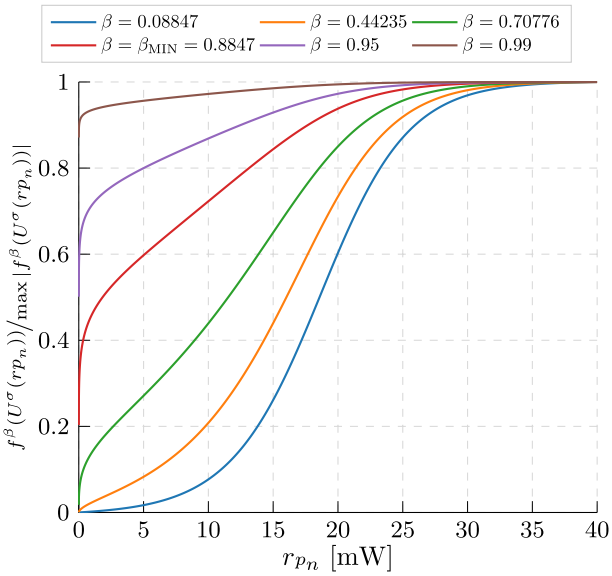


**Fig. 5** Scaled $f^\beta(U^\sigma(rp_n))$ for $1 > \beta > 0$ with $[a, b] = [300, 0.019]$

$$\begin{aligned}\hat{f}^\beta_{\text{lin}} &\triangleq \sum_{n=1}^{N} \frac{\partial \hat{f}^\beta}{\partial rp_n}\Big|_{\bar{rp}_n}(rp_n - \bar{rp}_n) + \frac{\partial \hat{f}^\beta}{\partial rd_n}\Big|_{\bar{rd}_n}(rd_n - \bar{rd}_n) + \hat{f}^\beta\left(\{\bar{rp}_n, \bar{rd}_n\}\forall_n\right) \\ &= \sum_{n=1}^{N} \frac{\hat{\mu} p_n}{(\bar{rp}_n)^\beta} \frac{ca\bar{\psi}_n}{(1+\bar{\psi}_n)^2} \frac{1-\alpha_n}{U^\sigma_{\text{MAX}}} rp_n + \frac{\hat{\mu} d_n}{(\bar{rd}_n)^\beta} \frac{\alpha_n}{R_{\text{MAX}}} rd_n + \text{Constant},\end{aligned} \tag{40}$$

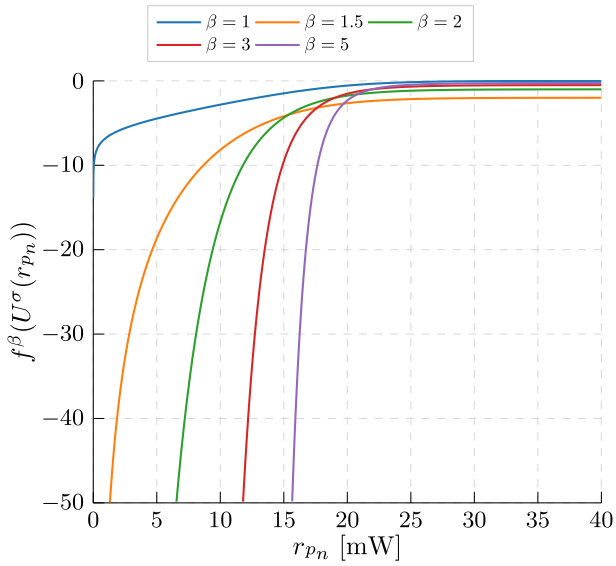


**Fig. 6** $f^{\beta}(U^{\sigma}(rp_n))$ for $\beta \geq 1$ with $[a, b] = [300, 0.019]$

where $\{\bar{r}p_n, \bar{r}d_n\}_{\forall n}$ is the set of rates and $\{\bar{\psi}_n\}_{\forall n}$ is the set of values for $\{\psi_n\}_{\forall n}$ achieved in the previous iteration. "Constant" represents all terms that are independent of $\{rp_n, rd_n\}_{\forall n}$ and so are constant. If these sets are updated according to

$$\begin{aligned} \ddot{r}d_{n_{i+1}} &= (1-\gamma_i)\ddot{r}d_{n_i} + \gamma_i rd_{n_i}, \\ \ddot{r}p_{n_{i+1}} &= (1-\gamma_i)\ddot{r}p_{n_i} + \gamma_i rp_{n_i}, \end{aligned} \tag{41}$$

and

$$\begin{aligned} \bar{\psi}_{n_{i+1}} &= e^{-a(\ddot{r}p_{n_{i+1}} - b)}, \\ \bar{r}d_{n_{i+1}} &= \frac{\alpha_n}{R_{\mathrm{MAX}}}\ddot{r}d_{n_{i+1}}, \\ \bar{r}p_{n_{i+1}} &= \frac{(1-\alpha_n)}{U^{\sigma}_{\mathrm{MAX}}}U^{\sigma}(\ddot{r}p_{n_{i+1}}), \end{aligned} \tag{42}$$

while the step size $\gamma$ is adjusted according to $\gamma_i = \frac{2}{2+i}$, then convergence is guaranteed [23]. Note that $\{rp_{n_i}, rd_{n_i}\}_{\forall n}$ is the solution in the $i$-th iteration and $\{\ddot{r}p_{n_{i+1}}, \ddot{r}d_{n_{i+1}}\}_{\forall n}$ is the $(i+1)$-th value defined by the exponential average in (41). Observe that for $i = 0, \gamma = 1$ and

$$\begin{aligned} \ddot{r}d_{n_1} &= rd_{n_0}, \\ \ddot{r}p_{n_1} &= rp_{n_0}. \end{aligned} \tag{43}$$

Replacing $\hat{f}^{\beta}$ with $\hat{f}^{\beta}_{\mathrm{lin}}$ in (18) and omitting the constant terms produces a problem that looks markedly like a weighted sum of rate and power maximization (WSRPM). Hence, the linearization enables interpreting the problem as a weighted sum given by

$$\begin{aligned} \underset{\{\mathsf{T}_k, \boldsymbol{s}_k\}\forall k}{\text{maximize}} \; & \sum_{n=1}^{N} \hat{w}p_n(1-\alpha_n)rp_n + \hat{w}d_n\alpha_n rd_n \\ \text{s.t.} \; & \sum_{n=1}^{N} p_n \leq P_{\text{Total}} \\ & s_{k,n} \geq 0 \quad \forall\, k, n \end{aligned}, \tag{44}$$

with weights

$$\begin{aligned} \hat{w}p_n &= \frac{\hat{\mu}p_n}{(\bar{r}p_n)^{\beta}} \frac{ca\psi_n}{(1+\psi_n)^2} \frac{1}{U^{\sigma}_{\text{MAX}}}, \\ \hat{w}d_n &= \frac{\hat{\mu}d_n}{(\bar{r}d_n)^{\beta}} \frac{1}{R_{\text{MAX}}}, \end{aligned} \tag{45}$$

for all users $n$.

## 4 Dual problem

Solving (18) directly is a challenging problem. It is computationally prohibitive because the computational complexity is exponential in $NK$ and the number of subcarriers $K$ can be large for practical implementations. This makes dual decomposition essential because it enables decomposing the problem into $K$ subproblems that can be solved in parallel, making the computational complexity linear in $NK$. Problem (18) compounds the issue because the $\alpha$-fairness utility functions as well as the sigmoidal-like function couple the subcarriers together and prevent direct decomposition. The linearization presented in Section 3.4, however, removes this hurdle by providing a means to sequentially solve (18) via (44), which can be decomposed. Moreover, casting (18) as the weighted sum in (44) enables easily utilizing the reasoning and methods developed in [7].

### 4.1 Dual problem formulation

Enabled by the time-sharing property of multicarrier systems, (44) can be solved to *near optimality* through Lagrange duality. The dual problem of (44) is formed by dualizing the total transmit power constraint. The Lagrange dual function is defined as

$$q(\boldsymbol{\alpha}, \hat{\boldsymbol{w}}p, \hat{\boldsymbol{w}}d, \lambda) \triangleq \max_{\mathsf{T},\mathsf{s}} \mathcal{L}(\boldsymbol{\alpha}, \hat{\boldsymbol{w}}p, \hat{\boldsymbol{w}}d, \lambda, \mathsf{s}, \mathsf{T}), \tag{46}$$

where $\lambda$ is the Lagrange multiplier for the total power constraint, $\boldsymbol{\alpha} = [\alpha_1, \ldots, \alpha_N]^{\top}$, $\hat{\boldsymbol{w}}p = [\hat{w}p_1, \ldots, \hat{w}p_N]^{\top}$, $\hat{\boldsymbol{w}}d = [\hat{w}d_1, \ldots, \hat{w}d_N]^{\top}$, and the Lagrangian is expressed as

$$\begin{aligned} &\mathcal{L}(\alpha, \hat{\boldsymbol{w}}p, \hat{\boldsymbol{w}}d, \lambda, \mathsf{s}, \mathsf{T}) \triangleq \lambda P_{\text{Total}} \\ &+ \sum_{k=1}^{K} \mathcal{L}^{\text{BC}}_k(\alpha, \hat{\boldsymbol{w}}p, \hat{\boldsymbol{w}}d, \lambda, \boldsymbol{s}_k, \mathsf{T}_k), \end{aligned} \tag{47}$$

where

$$\mathcal{L}_k^{\mathrm{BC}}(\boldsymbol{\alpha}, \hat{\boldsymbol{w}}p, \hat{\boldsymbol{w}}d, \lambda, \boldsymbol{s}_k, \mathsf{T}_k) = \sum_{n=1}^{N} \hat{w}d_n \alpha_n r d_n - \sum_{n=1}^{N} \boldsymbol{t}_{k,n}^{\mathcal{H}} \Upsilon_k(\boldsymbol{\alpha}, \hat{\boldsymbol{w}}p, \lambda) \boldsymbol{t}_{k,n} s_{k,n}, \tag{48}$$

and $\Upsilon_k(\boldsymbol{\alpha}, \hat{\boldsymbol{w}}p, \lambda)$ is given by

$$\Upsilon_k(\boldsymbol{\alpha}, \hat{\boldsymbol{w}}p, \lambda) \triangleq \left( \lambda \mathsf{I} - \sum_{m=1}^{N} \hat{w}p_m (1 - \alpha_m) \boldsymbol{h}_{k,m} \boldsymbol{h}_{k,m}^{\mathcal{H}} \right). \tag{49}$$

$\mathsf{I}$ is an $N_T \times N_T$ identity matrix. The Lagrange dual problem is then given by

$$\begin{aligned} &\underset{\lambda}{\text{minimize}}\ q(\boldsymbol{\alpha}, \hat{\boldsymbol{w}}p, \hat{\boldsymbol{w}}d, \lambda) \\ &\quad \text{s.t. } \lambda \geq 0 \\ &\qquad \Upsilon_k(\boldsymbol{\alpha}, \hat{\boldsymbol{w}}p, \lambda) \succ 0 \ \forall k \end{aligned}, \tag{50}$$

where the constraint on $\Upsilon_k(\boldsymbol{\alpha}, \hat{\boldsymbol{w}}p, \lambda)$ bounds (48).

### 4.2 Solving the dual problem

Observe that (50) is essentially the same as the dual problem developed in [7], where $\hat{w}p_n$ replaces the Lagrange multiplier $\lambda_n$ and $\hat{w}d_n$ replaces $\omega_n$ for all users $n$, and individual harvesting constraints are omitted. As such, the same methods can be used to solve for the power allocation and precoders. The optimal linear precoder is the minimum mean square error (MMSE) precoder because it balances interference suppression with power transfer, useful in the context of SWIPT, to maximize the SINR at a receiver. However, designing the MMSE precoder in the BC is a non-convex problem because the interference from signals intended for all other users, and consequently the associated precoders and power allocations, must be considered simultaneously. This can be overcome by using a MAC-BC duality which converts the per-subcarrier sub-problem from the BC to the dual MAC where the precoder, modeled as an equalizer, is only a function of the user dual power allocation on the particular subcarrier. The description of the process is minimized here for the sake of brevity, so refer to [7] for the details.

Applying a MAC-BC duality first involves equating the BC SINR in (5) to the dual MAC SINR (see [7]). With some algebraic manipulation, we have

$$\sum_{n=1}^{N} \boldsymbol{t}_{k,n}^{\mathcal{H}} \Upsilon_k(\boldsymbol{\alpha}, \hat{\boldsymbol{w}}p, \lambda) \boldsymbol{t}_{k,n} s_{k,n} = \boldsymbol{\sigma}_k^{\mathcal{H}} \boldsymbol{\delta}_k, \tag{51}$$

which relates the BC precoders and transmit powers to the dual MAC transmit powers. Note that on subcarrier $k$, $\boldsymbol{\sigma}_k$ and $\boldsymbol{\delta}_k$ are $N \times 1$ real-valued vectors of noise powers and dual MAC transmit powers, respectively, and $\Upsilon_k(\boldsymbol{\alpha}, \hat{\boldsymbol{w}}p, \lambda)$ is seen to act as a noise covariance matrix. Next, the MMSE equalizer can be found by maximizing the dual MAC SINR and is readily shown to be

$$\boldsymbol{t}_{k,n}^{*} = \left( \sum_{\substack{m=1 \\ m \neq n}}^{N} \delta_{k,m} \boldsymbol{h}_{k,m} \boldsymbol{h}_{k,m}^{\mathcal{H}} + \Upsilon_k(\boldsymbol{\alpha}, \hat{\boldsymbol{w}}p, \lambda) \right)^{-1} \boldsymbol{h}_{k,n}. \tag{52}$$

The equalizer in (52) will be used as a precoder in the BC. The expression in (52) enables the dual MAC SINR to be expressed as only a function of $\boldsymbol{\delta}_k$,

$$\gamma_{k,n}^{\mathrm{MAC}}(\boldsymbol{\delta}_k) = \delta_{k,n} \boldsymbol{h}_{k,n}^{\mathcal{H}} \left[ \sum_{\substack{m=1 \\ m \neq n}}^{N} \delta_{k,m} \boldsymbol{h}_{k,m} \boldsymbol{h}_{k,m}^{\mathcal{H}} + \Upsilon_k(\boldsymbol{\alpha}, \hat{\boldsymbol{w}}p, \lambda) \right]^{-1} \boldsymbol{h}_{k,n}. \tag{53}$$

The maximization in (46) can now be reformulated as only a function of the dual MAC transmit powers through (51) and by replacing the BC SINR with (53).

The problem is still non-convex and successive convex approximation (SCA) may be employed to calculate the dual MAC transmit powers. This is done by fixing constant the dual MAC transmit powers $\delta_{k,m}$ for all $m \neq n$, denoted with $\bar{\delta}_{k,m}$, and approximating the respective dual MAC data rates with their first-order Taylor expansion. KKT conditions enable calculating the optimal value for the dual MAC transmit power, $\delta_{k,n}$, via the following equation:

$$\delta_{k,n}^{*} = \left[ 0, \frac{\hat{w} p_n \alpha_n}{\ln(2)(\bar{\phi}_{k,n} + \sigma_{k,n})} - \frac{1}{\bar{q}_{k,n}} \right]^{+}, \tag{54}$$

where $[x, ..., y]^{+} = \max\{x, ..., y\}$, $\bar{q}_{k,n}$ is the interference-plus-noise covariance,

$$\bar{q}_{k,n} = \boldsymbol{h}_{k,n}^{\mathcal{H}} \left[ \sum_{\substack{m=1 \\ m \neq n}}^{N} \bar{\delta}_{k,m} \boldsymbol{h}_{k,m} \boldsymbol{h}_{k,m}^{\mathcal{H}} + \Upsilon_k(\boldsymbol{\alpha}, \hat{\boldsymbol{w}}p, \lambda) \right]^{-1} \boldsymbol{h}_{k,n}, \tag{55}$$

and $\bar{\phi}_{k,n}$ is from the first-order Taylor series expansion of the data rates,

$$-\bar{\phi}_{k,n} = \frac{\partial}{\partial \delta_k} \left[ \sum_{\substack{m=1 \\ m \neq n}}^{N} \hat{w} d_m \alpha_m \log_2(1 + \gamma_{k,m}^{\mathrm{MAC}}(\boldsymbol{\delta}_k)) \right] \Bigg|_{\boldsymbol{\delta}_k = \bar{\boldsymbol{\delta}}_k}. \tag{56}$$

## 5 Algorithm

Algorithm 1 describes the procedure for solving (18) through a sequential linearization where each problem iterate is defined in (44) with weights defined in (45). For each weight iterate, a bisection algorithm is used to adjust the Lagrange multiplier $\lambda$ until the total transmit power constraint is met. For each iterate of $\lambda$, the SCA in [7] is used to determine the power allocation and the beamforming vectors. Once the total

transmit power constraint is met tightly, the resource allocation is checked for convergence; otherwise, the weights (45) are updated and the process continues.

Due to the constraint on $\Upsilon_k(\boldsymbol{\alpha}, \hat{\boldsymbol{w}}p, \lambda)$, the lower bound $\lambda_{\text{MIN}}$ for $\lambda$ is given by the maximum eigenvalue of $\mathsf{H}_k{}^{\mathcal{H}} diag(\hat{\boldsymbol{w}}p \circ (1-\boldsymbol{\alpha}))\mathsf{H}_k$ over all subcarriers $k$, where $\circ$ is the Hadamard product. The upper bound $\lambda_{\text{MAX}}$ for $\lambda$ is any value greater than $\lambda_{\text{MIN}}$ that causes (50) to satisfy the total transmit power constraint, i.e.,

$$\sum_{n=1}^{N} p_n \leq P_{\text{Total}}. \tag{57}$$

$\lambda_{\text{MAX}}$ can be found by iteratively solving (50) while simultaneously increasing (e.g., doubling) $\lambda$ until the total transmit power constraint is satisfied, starting with $\lambda > \lambda_{\text{MIN}}$. Once the bounds are found, a bisection is used to find the optimal value for $\lambda$.

**Algorithm 1** $\alpha$-Fair resource allocation

Choose $\alpha_n \in [0,1]\ \forall\ n$, $\{\hat{\mu}_{p_n}, \hat{\mu}_{d_n}\}_{\forall n}$, and $\beta > \beta_{\text{MIN}}$
Choose convergence tolerances $\epsilon_p$ $\epsilon_\beta$
$i = 0, \hat{\boldsymbol{w}}_{p_i} = \hat{\boldsymbol{\mu}}_p$, $\hat{\boldsymbol{w}}_{d_i} = \hat{\boldsymbol{\mu}}_d$
Initialize $\{\ddot{r}_{p_{n_i}}, \ddot{r}_{d_{n_i}}\}_{\forall n} = 0$
**while** true **do** ▷ Sequential Linearization
  Choose $\lambda_{\text{MIN}}, \lambda_{\text{MAX}}$
  $j = 0$, $\Delta_p = \infty$
  **while** $\Delta_p \geq \epsilon_p$ **do** ▷ Total Power Constraint
    $\lambda_j = (\lambda_{\text{MAX}} + \lambda_{\text{MIN}})/2$
    $\{\mathsf{T}_j, \mathsf{s}_j\} = \text{SCA}(\hat{\boldsymbol{w}}_{p_i}, \hat{\boldsymbol{w}}_{d_i}, \lambda_j, \mathsf{H}, \boldsymbol{\sigma})$ from [7]
    Calculate $p_{n_j}$ $\forall n$ with (8) then $P_j = \sum_n^N p_{n_j}$
    **if** $P_j < P_{\text{Total}}$ **then**
      $\lambda_{\text{MAX}} = \lambda_j$
    **else**
      $\lambda_{\text{MIN}} = \lambda_j$
    **end if**
    $\Delta_p = {}^{|P_j - P_{\text{Total}}|}/_{P_{\text{Total}}}$, $j = j + 1$
  **end while**
  Generate $\{r_{p_{n_i}}, r_{d_{n_i}}\}_{\forall n}$ using (4) and (7)
  Update $\gamma_i = {}^{2}/_{2+i}$
  Update $\ddot{\boldsymbol{r}}_{i+1} = \{\ddot{r}_{p_{n_{i+1}}}, \ddot{r}_{d_{n_{i+1}}}\}_{\forall n}$ using (41)
  **if** $\left\| \frac{\ddot{\boldsymbol{r}}_{i+1} - \ddot{\boldsymbol{r}}_i}{\ddot{\boldsymbol{r}}_{i+1} + \ddot{\boldsymbol{r}}_i} \right\| \leq \epsilon_\beta$ **then**
    **return** $\{\hat{\boldsymbol{w}}_{p_i}, \hat{\boldsymbol{w}}_{d_i}, \{r_{p_{n_i}}, r_{d_{n_i}}\}_{\forall n}, \mathsf{T}_i, \mathsf{s}_i, P_i, \lambda_i\}$
  **end if**
  Update $\{\bar{r}_{p_{n_{i+1}}}, \bar{r}_{p_{n_{i+1}}}\}_{\forall n}$ and $\{\bar{\psi}_{n_{i+1}}\}_{\forall n}$ using (42)
  $i = i + 1$
  Calculate $\hat{\boldsymbol{w}}_{p_i}$, $\hat{\boldsymbol{w}}_{d_i}$ from (45) ▷ Update the weights
**end while**

### 5.1 Asymptotic computational complexity

Asymptotic computational complexity is utilized to describe how the computational complexity grows w.r.t. input size and the algorithm.

#### 5.1.1 SCA

The SCA is implemented in [7] which utilizes one of two updating methods, serial updating (Gauss-Seidel) or parallel updating (Jacobi). The matrix inversion in (55) normally has complexity $O\left(N_T^3\right)$ but can be reduced to $O\left(N_T^2\right)$ by using the Sherman-Morison identity [24] and rank-1 updates. Consequently, the power allocation portion of these algorithms has asymptotic computational complexity $O\left(KN_T^2N\epsilon_\delta^{-1}\right)$ with tolerance $\epsilon_\delta$ if using serial updating or $O\left(KN_T^2\right)$ which normally converges within 10 iterations if using parallel updating [7].

#### 5.1.2 Total transmit power

(44) only has a total transmit power constraint. With only one constraint, Algorithm 1 uses a bisection algorithm to find the Lagrange multiplier. Bisection converges within $O\left(\log_2((\lambda_{\text{MAX}}-\rho_{\text{MAX}})\epsilon_p^{-1})\right)$ iterations [25], where $\rho_{\text{MAX}}$ is the largest eigenvalue of $\mathsf{H}_k{}^{\mathcal{H}}diag(\hat{\boldsymbol{w}}p\circ(1-\boldsymbol{\alpha}))\mathsf{H}_k$ over all subcarriers $k$ and $\epsilon_p$ is the tolerance for the total transmit power constraint.

#### 5.1.3 $\alpha$-fairness utility

Given $\{\hat{\mu}p_n,\hat{\mu}d_n\}_{\forall n}$, $\boldsymbol{\alpha}$, and $\beta$, Algorithm 1 utilizes the conditional gradient method to solve a series of weighted sum of data rate and power maximizations for successive weight iterates until convergence to find the optimal resource allocation. It solves a sequence of linearized sub-problems using a diminishing step size which converges within $O\left(\epsilon_\beta^{-1}\right)$ iterations [23], where $\epsilon_\beta$ is the tolerance. Each iteration has $O\left(max(N^2K(N_T+1),N\ln(\beta))\right)$computational complexity.

#### 5.1.4 Comparison to the standard method

A common approach to addressing the non-convexity of the sigmoidal-like function, as proposed in [15], involves transforming the sum of sigmoidal-like functions problem into a parametric subtractive form that is convex. This iterative method uses a damped Newton step, achieving optimality with linear convergence initially and superlinear convergence near the solution. In contrast, the conditional gradient method applied to the concave utility converges sublinearly (i.e., $O\left(\epsilon_\beta^{-1}\right)$ but with significantly lower computational complexity per iteration, as it avoids the matrix inversion required in the Newton step. Furthermore, the use of $\alpha$-fairness utility functions in this work was not merely to simplify the integration of nonlinear harvesting effects, but to generalize the problem to a relative resource allocation that incorporates fairness across objectives, rather than focusing solely on power harvesting constraints. If the transformation from [15] were adopted here, it would introduce an additional loop to adjust the transformed problem's parameters. However, this paper demonstrates that such a transformation is unnecessary when sigmoidal-like functions are paired with $\alpha$-fairness utility functions and an appropriate fairness value is used.

### 5.2 Optimality

Since the objective $\hat{f}^\beta$, is concave provided $\beta>\beta_{\text{MIN}}$, and the domain of (18) is convex due to time-sharing, successive linearization—where the problem is solved by

optimizing the linearized version at successive iterates—should result in the globally optimal solution. Each linear problem is weighted by the tangent of the nonlinear problem at the current iterate. When the tangent has zero slope, a critical point has been reached, which, for concave functions, is the global maximum. At this point, the linear problem can no longer improve the objective. Hence, (18) can be solved iteratively through linearization by repeatedly solving (44) for each update to the weights defined in (45). However, the underlying power allocation problem is still non-convex due to the nature of multiuser power allocations on individual subcarriers, so only a locally optimal solution is guaranteed. Since each subcarrier contributes only a small amount to the total objective, the suboptimality may be minor, especially if many subcarriers reach globally optimal solutions.

## 6 Results and discussion

### 6.1 Comments on general application

The authors in [21] showed that when a proportionally fair (i.e., $\beta = 1$) utility function encapsulates a sigmoidal-like function, the resulting composite function is concave w.r.t. to the input of the sigmoidal-like function. It is a convenient feature, but also restricts the resulting output to proportionally fair. This paper generalized this particular result by specifically defining the range of fairness values ($\beta > \beta_{\text{MIN}}$) that make a sigmoidal-like function encapsulated by an $\alpha$-fair utility function concave. Since $2\sqrt{e^{ab}}(1+e^{ab})^{-1} > 0$, the $\max(\beta_{\text{MIN}}) < 1$, so the most amount of fairness required for the situation is approximately proportionally fair or $\beta = 1$. With convenient values of $a$ and $b$, the fairness criterion may be reduced further. Also, note that it is possible to have different fairness values based on the objective, so $\beta d > 0$ could be used for the data rates while $\beta p > 1 - 2\sqrt{e^{ab}}(1+e^{ab})^{-1}$ for harvested power. Indeed, setting $\beta p$ to be large while $\beta d$ is small might be a convenient way to have a greedier data rate allocation while ensuring that all users harvest a reasonable amount of power.

Concerning the sigmoidal-like harvesting model, directly incorporating it into an optimization requires a transformation due to its non-concavity. Hence, encapsulating the harvesting model in an $\alpha$-fair utility function is a novel and easy alternative. In addition, linearization offers the means to apply the model to generic WSRPMs. The linearization of the composite utility w.r.t. to the underlying resource allocation results in a WSRPM as demonstrated in (40) and, since the linearization is agnostic to the system model and methods used to determine $\{rp_n, rd_n\}_{\forall n}$, it can be applied generically.

### 6.2 Simulations

The common parameters used for the following simulations are listed in Table 1. Note that only one set of time-switching ratios is used since they are constant in these simulations and the particular values merely limit the range of user data rates and harvested powers. SWIPT related research has studied a range of carrier frequencies from 900 MHz [28] to 2.4 GHz [29] to higher frequencies associated with 5G communications [30]. In this paper, the number of subcarriers and channel bandwidth is based on WiFi, since WiFi is a ubiquitous wireless technology that utilizes OFDM, while the carrier frequency is set to 915 MHz which is in an unlicensed industrial, scientific, and medical (ISM) band. The MISO channel matrix $\mathsf{H}$ is generated using the MATLAB

**Table 1** System parameters

| Parameter | Value |
|---|---|
| First Subcarrier Frequency, $f_0$ | 915 MHz |
| Number of Subcarriers,$K$ | 64 |
| Subcarrier Bandwidth | 312500 Hz |
| OFDM Passband Bandwidth | 20 MHz |
| Total Power Constraint, $P_{\text{Total}}$ | 30 dBm |
| Large Scale Path Loss, $P_{\text{LOS}}$ | 27 and 47 dB |
| Number of Transmit Antennas, $N_T$ | 10 |
| Number of Users, $N$ | 2, 4 |
| Time-Switching Ratio, $\boldsymbol{\alpha}^n$ | 0.5 |
| Fading Environment | Rician [26], Model B |
| K-factor | 3 |
| Noise Power Density, $\sigma$ | -112 dBm /Hz |
| Saturation Power, $P_{\text{SAT}}$ | 24 mW and 10 $\mu$ W |
| Convergence Tolerance, $\epsilon_\beta$ | $1e-4$ |
| Convergence Tolerance, $\epsilon_p$ | $1e-7$ |

The path loss values are chosen not as typical values seen in a practical wireless power harvesting situation, but to highlight the functionality of the algorithm by ensuring the power harvester is in saturation

**Table 2** MIMOChannel toolbox settings

| Parameter | Value |
|---|---|
| 'SampleRate' | 20 MHz |
| 'SpatialCorrelationSpecification' | 'None' |
| 'NumTransmitAntennas' | $N_T$ |
| 'NumReceiveAntennas' | $N$ |
| 'FadingDistribution' | 'Rician' |
| 'KFactor' | 3 |
| 'MaximumDopplerShift' | 0 |
| 'NormalizeChannelOutputs' | true |
| 'AntennaSelection' | 'Tx and Rx' |

communications toolbox [31] using the settings in Table 2 in conjunction with a tapped delay line model specified in [26]. The channel impulse response is first attained for each transmit-receive antenna pair and a fast Fourier transform (FFT) is used to attain the individual channel vectors for each user $n$ on each subcarrier $k$ given by $\boldsymbol{h}_{k,n}$. The channel vectors are then kept constant for simulations with the same parameters (i.e., $K$, $N$, $N_T$, etc.), but are updated when the system changes.

Problems (18) and (44) are non-convex when $N \geq 2$. The reader is referred to [7] for simulations with $2 \leq N \leq 7$ using the underlying optimization method used here to solve (44) (and consequently (18)). In this section, two-user and four-user networks are used to demonstrate the application of the composite utility to incorporate the nonlinear power harvesting effects. Table 3 lists the parameters used to examine the impact of the power harvesting model. Three power harvesting models are used. The first model, [150, 0.014] from [27], is slightly non-convex and the second, [300, 0.019], further emphasis the non-convexity. The third model, [15000, 1e−6] from [15], is

**Table 3** Harvested power parameters

| Parameter | Value |
|---|---|
| $[a, b]$ | [150, 0.014] [27] [300, 0.019] [15000, 1e−6][15] |
| $\hat{\boldsymbol{\mu}}_p$ | $[10, 2]^\top [10, 2, 1, 1]^\top$ |
| $\hat{\boldsymbol{\mu}}_d$ | $[1, 1]^\top [1, 1, 1, 1]^\top$ |

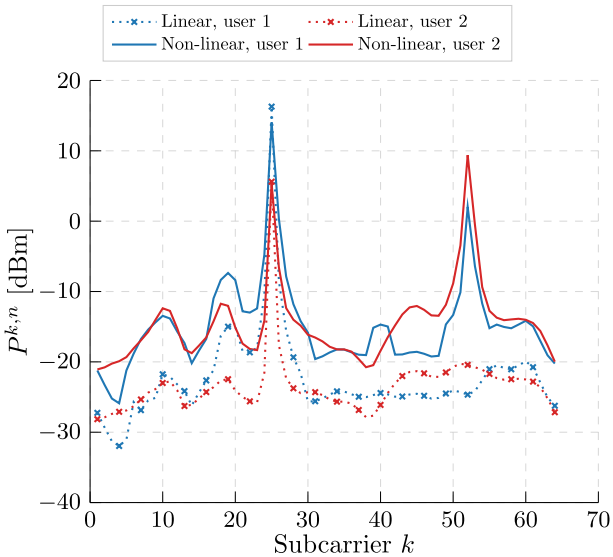


**Fig. 7** The received power with $N = 2$, $P_{\text{LOS}} = 27$ dB, $P_{\text{SAT}} = 24$mW, $[a, b] = [150, 0.014]$, $\beta_{\text{MIN}} = 0.3764$, $\beta = 0.3802$, and $\eta = 0.75218$

designed for a more realistic scenario in which the received power and consequently the harvester output power are much smaller due to a larger transmission range. The efficiency of the linear model is set to the efficiency of the nonlinear model at its inflection point. The inflection point is given by the parameter $b$, so the efficiency $\eta$ can be calculated through

$$\eta = \frac{U^{\sigma}(b) P_{\text{SAT}}}{b}. \tag{58}$$

The following figures illustrate the impact of the harvesting model on the received power allocation and the harvester output power at each user. Specifically, Figs. 7, 9, and 11 illustrate the power received by each user w.r.t. the subcarrier. Figures 8, 10, and 12 illustrate the harvester output power before applying the time-switching ratio as a function of the received power summed over all subcarriers for each user. For simplicity, it is assumed that each user utilizes the same harvester in each figure. In addition, the nonlinear model is considered accurate as it is envisioned that the parameters are fit to the characteristics of the actual harvester circuits (e.g., [15,

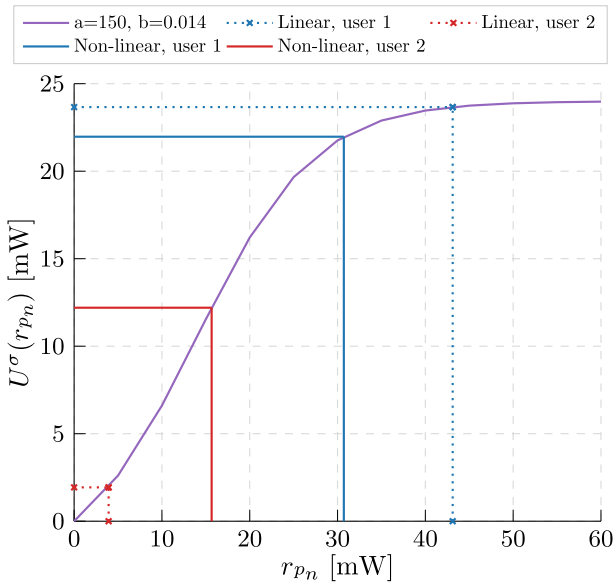


**Fig. 8** The harvester output power with $N = 2$, $P_{\text{LOS}} = 27$ dB, $P_{\text{SAT}} = 24$mW, $[a, b] = [150, 0.014]$, $\beta_{\text{MIN}} = 0.3764$, $\beta = 0.3802$, and $\eta = 0.75218$

27]), while the linear model is merely a constant efficiency. To compare the harvester output power for the different models, the nonlinear model is applied to the resulting received power for both models to generate the actual output power. Lastly, the fairness value $\beta$ is chosen to be slightly greater than $\beta_{\text{MIN}}$ to ensure the concavity of the objective while encouraging nearly a minimal amount of fairness between the objectives.

The impact of the harvesting model on the received power for each user in the two-user network is illustrated in Fig. 7 for a fairness value of $\beta = 0.3802$, slightly greater than $\beta_{\text{MIN}} = 0.3764$. Observe that the nonlinear harvesting model produces a higher subcarrier power allocation than the linear harvesting model for all subcarriers except for $k = 25$, which is where the peak power allocation for both models occurs. The nonlinear power harvesting model has a saturation point where additional input power has a reduced ability to increase the output power and encourages the optimization to allocate power elsewhere, resulting in the higher general subcarrier power allocation but a lower peak power allocation on $k = 25$.

The purple trace labeled $a = 150, b = 0.014$ in Fig. 8 illustrates the output power (y-axis) of the nonlinear harvester as a function of the received power (x-axis). Observe that the curve begins to saturate at roughly 20 mW and fully saturates by 50 mW. The impact on the harvester output power for the received powers illustrated in Fig. 7 for each user (summed over all subcarriers) is also illustrated in Fig. 8. Notice that when the nonlinear harvesting model is used, the received power for user 1 is reduced from 43 mW to 30.7 mW, but only results in a reduction of roughly 1.7 mW in DC power. This reduction in the power allocated to user 1 is used to increase the data rates for both users by increasing the general subcarrier power allocation as seen in Fig. 7, as well as the harvester output power for user 2 which roughly increases from 1.9 mW to 12 mW. The impact of the harvesting models and network size on

**Table 4** Time-switched spectral efficiency, $\tilde{r}d_n$

| Parameters | user 1 bpsHz$^{-1}$ | user 2 bpsHz$^{-1}$ | user 3 bpsHz$^{-1}$ | user 4 bpsHz$^{-1}$ | Network bpsHz$^{-1}$ |
|---|---|---|---|---|---|
| $N = 2$ Linear, $\eta = 0.75218$ | 5.75 | 4.26 | - | - | 10.03 |
| $N = 2[a, b] = [150, 0.014]$ | 7 | 3.67 | - | - | 10.67 |
| $N = 4$ Linear, $\eta = 0.75218$ | 5.67 | 4.76 | 4.37 | 4.26 | 19.10 |
| $N = 4[a, b] = [150, 0.014]$ | 6.68 | 4.96 | 4.51 | 4.51 | 20.70 |
| $N = 4$ Linear, $\eta = 0.62947$ | 5.81 | 4.70 | 4.39 | 4.14 | 19.04 |
| $N = 4[a, b] = [300, 0.019]$ | 6.20 | 4.73 | 4.21 | 4.03 | 19.2 |

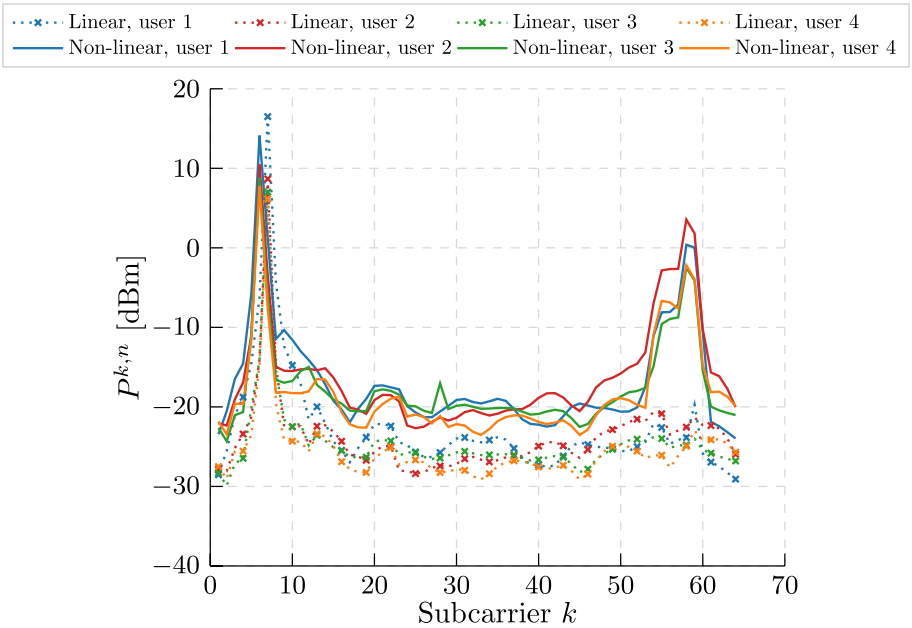


**Fig. 9** The received power with $N = 4$, $P_{\text{LOS}} = 27$ dB, $P_{\text{SAT}} = 24$mW, $[a, b] = [150, 0.014]$, $\beta_{\text{MIN}} = 0.3764$, $\beta = 0.3802$, and $\eta = 0.75218$

the time-switched user data rates (i.e., $\tilde{r}d_n$ for user $n$) is described in Table 4. Moving from a linear harvesting model to a nonlinear model increases the network data rate from 10.03 bpsHz$^{-1}$ to 10.67 bpsHz$^{-1}$.

Figure 9 illustrates the impact of the harvesting model on the received power for each user in the four-user network for the same power harvesting model as in Fig. 7. Similar to the two-user network, most of the subcarriers in the four-user network show an increase in received power when using the nonlinear model. The peak received power allocated to $k = [6, 7]$, in the linear model is reduced to only $k = 6$ in the nonlinear model. The nonlinear model also produces a smaller second received power peak for $53 \leq k \leq 60$ that is not produced by the linear model. Figure 10 shows the impact on the harvester output power. Similar to the two-user network, the harvester output power for user 2 in the four-user network increased by 10 mW. The harvester output power for user 3 and user 4 also increased when using the nonlinear harvesting model. Table 4

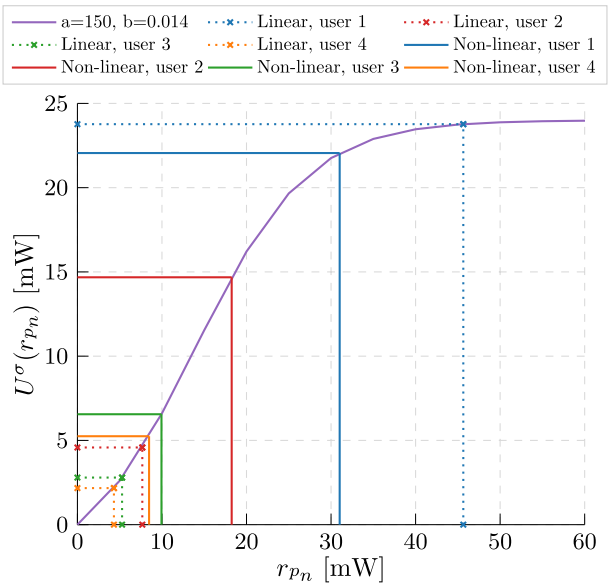


**Fig. 10** The harvester output power with $N = 4$, $P_{\text{LOS}} = 27$ dB, $P_{\text{SAT}} = 24$mW, $[a, b] = [150, 0.014]$, $\beta_{\text{MIN}} = 0.3764$, $\beta = 0.3802$, and $\eta = 0.75218$

shows the nonlinear model increases the network data rate from 19.10 bpsHz$^{-1}$ to 20.70 bpsHz$^{-1}$.

Figure 11 illustrates the impact of a more non-convex harvesting model, specifically $[a, b] = [300, 0.019]$, on the received power for each user in the four-user network. It is similar to Fig. 9, but there is more power allocated to the second peak located at

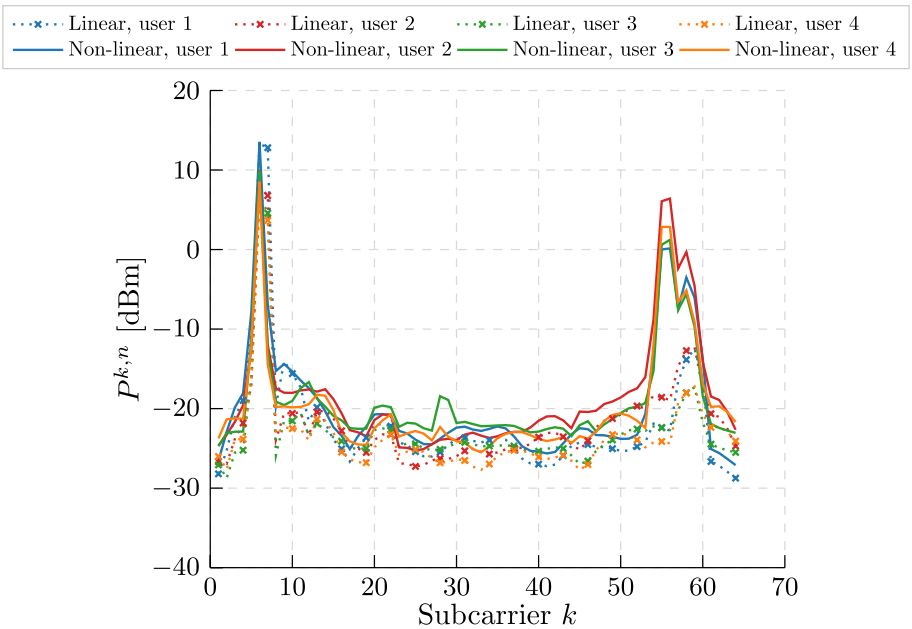


**Fig. 11** The received power with $N = 4$, $P_{\text{LOS}} = 27$ dB, $P_{\text{SAT}} = 24$mW, $[a, b] = [300, 0.019]$, $\beta_{\text{MIN}} = 0.8846$, $\beta = 0.8935$, and $\eta = 0.62947$

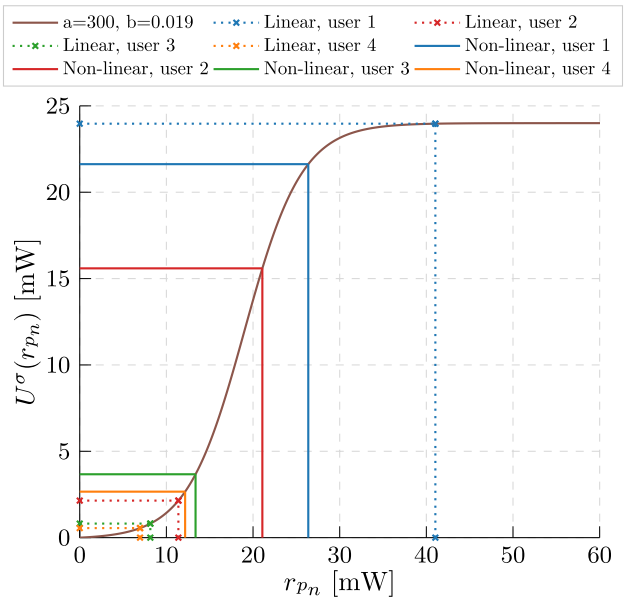


**Fig. 12** The harvester output power with $N = 4$, $P_{\text{LOS}} = 27$ dB, $P_{\text{SAT}} = 24$mW, $[a, b] = [300, 0.019]$, $\beta_{\text{MIN}} = 0.8846$, $\beta = 0.8935$, and $\eta = 0.62947$

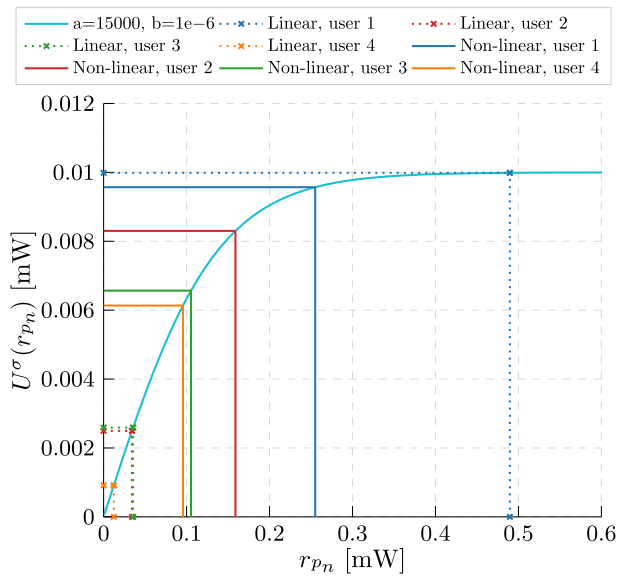


**Fig. 13** Harvester output power with $N = 4$, $P_{\text{LOS}} = 47$ dB, $P_{\text{SAT}} = 10\,\mu$W, $[a, b] = [15000, 1\text{e}{-6}]$, $\beta_{\text{MIN}} = 2.81\text{e}{-5}$, $\beta = 2.8410\text{e}{-5}$, and $\eta = 0.07444$

subcarrier $k = 55$. Figure 12 illustrates the resulting harvester output powers. The harvester output power achieved by user 1 is roughly the same as that in Fig. 10, but with a lower received power. However, the harvester output power achieved by user 2 increased by roughly 13 mW compared to the linear harvesting model and is about 3 mW more than Fig. 10. This is likely due to the higher turn-on power of the circuit and the steeper charging rate having reduced the amount of received power user 1 required to produce the same harvester output power. Table 4 shows the nonlinear model increases

**Table 5** Fairness simulation parameters

| Parameter | Value |
|---|---|
| $P_{\text{SAT}}$ | 10 μW |
| $P_{\text{LOS}}$ | 47 dB |
| $[a, b]$ | [15000, 1e−6][15] |
| $\hat{\boldsymbol{\mu}}_p$ | $[10, 2, 1, 1]^\top$ |
| $\hat{\boldsymbol{\mu}}_d$ | $[10, 1, 2, 1]^\top$ |

the network data rate from 19.04 bpsHz$^{-1}$ to 19.2 bpsHz$^{-1}$. If a lower harvester output power is acceptable, the range of the system can be increased for the same transmission parameters. Figure 13, for example, illustrates a scenario in which the signal is attenuated by 47 dB, corresponding to about a 6 m range, and produces up to 10 μ W. The nonlinear power harvester model used here is based on circuit data presented in [15].

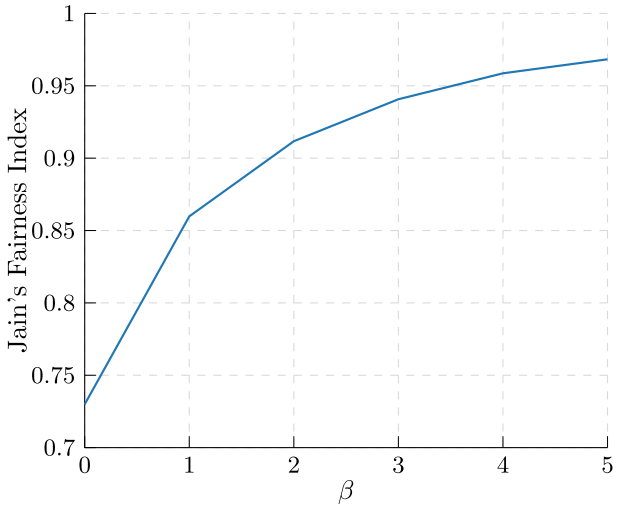


**Fig. 14** Jain's fairness index as a function of the fairness parameter

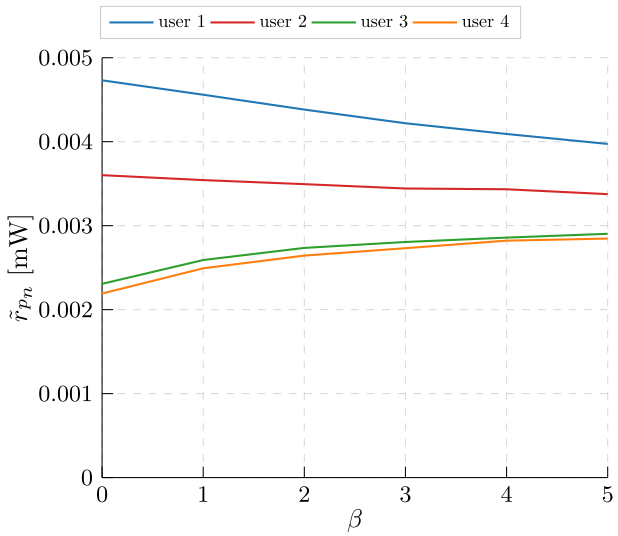


**Fig. 15** Time-switched harvested power as a function of the fairness parameter

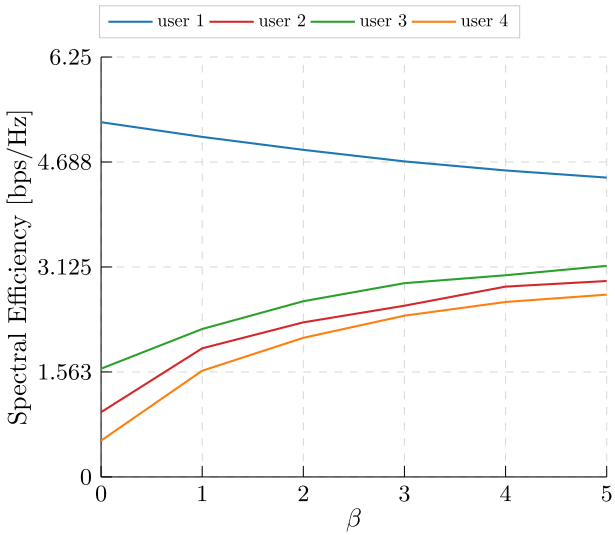


**Fig. 16** The time-switched user spectral efficiency as a function of the fairness parameter

Table 5 lists the parameters used to examine fairness between the objectives in a four-user network. Figures 14, 15, and 16 show the impact of the fairness parameter $\beta$ on the fairness of the resource allocation, harvester output power, and the data rate, respectively. Fairness is measured using Jain's fairness index [32]. There are $2N$ objectives, so the index ranges from $\frac{1}{2N}$ to 1, where 1 means all users have the same allocation. As expected, fairness increases with $\beta$ in Fig. 14. Harvested power became increasingly equitable between the users as $\beta$ increased in Fig. 15. Likewise, in Fig. 16 the data rates became increasingly equitable as $\beta$ increased.

### 6.3 Practical implementation considerations

One use-case in which SWIPT may be a practical solution is wireless sensing in challenging locations (e.g., rotating machinery, embedded in physical structures, etc.). Wireless sensors already emphasize low-power consumption, so the lower power transfer efficiency of far-field power transfer is less of a hindrance. Furthermore, challenging deployment locations make maintenance, in particular battery maintenance, difficult or even impossible and consequently expensive. Hence, there is an incentive to wirelessly power these devices. In such a scenario, one standard that could utilize the ideas presented in this paper is WiFi since it is a ubiquitous OFDM-based technology that supports multiantenna multiuser wireless networks and is already utilized by some wireless sensing technologies.

To incorporate the presented algorithm into WiFi, it is envisioned that connecting devices would report the harvester coefficients they have stored (parameters $a$ and $b$) to the access point. These values are determined at the factory through curve fitting. Based on the collection of harvesters in the network and the resource allocation fairness requirements, the access point would run the algorithm to calculate the precoding vectors and the power allocation. The algorithm would need to exclude certain subcarriers since a few will be used as pilot tones to determine the channel coefficients as well as utilize an appropriate system-specific total transmit power constraint. The resulting

power allocation, given by $\{s_k\}_{\forall k}$, amounts to a scaling that is applied to the QAM symbols as they are transmitted. The network resource allocation is periodically updated based on the weights $\{\hat{\mu}p_n, \hat{\mu}d_n\}_{\forall n}$, which reflect the evolution of the data queues and battery states. In addition, many wireless devices must adhere to power spectral density transmission limits, which was not addressed here but could be incorporated by adding additional constraints to the resource allocation problem.

## 7 Conclusion

Recent research in [7] proposed a novel near-optimal resource allocation method for a multiantenna MU SWIPT network that employs OFDM. However, it employed a MAC-BC duality that necessitated using a linear power harvesting model, disregarding the nonlinear nature of power harvesting in SWIPT networks. This paper addresses this issue by incorporating nonlinear power harvesting effects through a power harvesting model based on sigmoidal-like functions. Sigmoidal-like functions, being neither convex nor concave, typically necessitate transformation for tractability, a challenge compounded by the MAC-BC duality. We propose an alternate approach in which a parameterized class of utility functions known as $\alpha$-fairness is used to generalize the SWIPT resource allocation problem and concavify the nonlinear power harvesting model. Inspired by [21], this paper shows that the composite utility is strictly concave for fairness parameters greater than a certain value related to the harvesting model and improves on [21] by enabling a much wider range of fairness. This methodology is then used to simplify the integration of nonlinear effects across a broad spectrum of fairness values into the considered problem. Since the composite utility is strictly concave, the relatively complex procedure used in [15] is unneeded. Moreover, the application of the composite utility was readily demonstrated by linearizing and iteratively maximizing it using the resource allocation in [7] which relied on a linear harvesting model, in effect adding the nonlinear power harvesting model to the existing algorithm.

**Author Contributions**
All work was produced by RK under the supervision of MM. All authors read and approved the final manuscript.

**Funding**
This work was supported by Fonds de la Recherche Scientifique-FNRS and the Fonds Wetenschappelijk Onderzoek-Vlaanderen under EOS Project no 30452698 '(MUSE-WINET) MUlti-SErvice WIreless NETwork' and FWO Research Project nr. G0C0623N "User-centric distributed signal processing algorithms for next-generation cell-free massive MIMO-based wireless communication networks".

**Availability of Data and Materials**
The datasets used and/or analyzed during the current study are available from the corresponding author on reasonable request.

## Declarations

**Competing interests**
There are no competing interests.

Received: 13 June 2024 Accepted: 16 November 2024
Published online: 03 March 2025

**References**


1. L. R. Varshney. Transporting information and energy simultaneously. In: Proceedings of the IEEE International Symposium on Information Theory, Toronto, Canada, pp. 1612–1616 (2008). https://doi.org/10.1109/ISIT.2008.4595260
2. P. Grover, A. Sahai, Shannon meets Tesla: Wireless information and power transfer. In: 2010 IEEE International Symposium on Information Theory, Austin, TX, USA, pp. 2363–2367 (2010). https://doi.org/10.1109/ISIT.2010.5513714
3. R. Zhang, C.K. Ho, MIMO broadcasting for simultaneous wireless information and power transfer. in IEEE Transactions on Wireless Communications, vol. 12, no. 5, pp. 1989-2001, May 2013, https://doi.org/10.1109/TWC.2013.031813.120224
4. X. Lu, P. Wang, D. Niyato, D.I. Kim, Z. Han, Wireless networks with RF energy harvesting: a contemporary survey. in IEEE Communications Surveys & Tutorials, vol. 17, no. 2, pp. 757-789, Second quarter 2015, https://doi.org/10.1109/COMST.2014.2368999
5. S. Hayashi, Z.-Q. Luo, Dynamic Spectrum Management: When is FDMA Sum-Rate Optimal? In: 2007 IEEE International Conference on Acoustics, Speech and Signal Processing - ICASSP '07, Honolulu, HI, USA, 2007, pp. III-609-III-612, https://doi.org/10.1109/ICASSP.2007.366753
6. E. Björnson, M. Bengtsson, B. Ottersten, Optimal multiuser transmit beamforming: a difficult problem with a simple solution structure [lecture notes]. IEEE Signal. Process. Magaz. **31**(4), 142–148 (2014). https://doi.org/10.1109/MSP.2014.2312183
7. R.P. Ketcham, J. Verdyck, M. Moonen, Joint beamforming and power allocation for multiuser miso broadcast channel SWIPT employing OFDM. IEEE Access **9**, 165154–165172 (2021). https://doi.org/10.1109/ACCESS.2021.3132769
8. Y. Wei, R. Lui, Dual methods for nonconvex spectrum optimization of multicarrier systems. IEEE Trans. Commun. **54**(7), 1310–1322 (2006). https://doi.org/10.1109/TCOMM.2006.877962
9. Z. Luo, S. Zhang, Dynamic spectrum management: complexity and duality. IEEE J. Select. Top. Signal Process. **2**(1), 57–73 (2008). https://doi.org/10.1109/JSTSP.2007.914876
10. B. Clerckx, R. Zhang, R. Schober, D.W.K. Ng, D.I. Kim, H.V. Poor, Fundamentals of wireless information and power transfer: from rf energy harvester models to signal and system designs. IEEE J. Select. Area. Commun. **37**(1), 4–33 (2019). https://doi.org/10.1109/JSAC.2018.2872615
11. S. Wang, L. Ma, W. Wu, Joint TS beamforming and hybrid TS-PS receiving design for SWIPT systems. IEEE Access. **9**, 50686–50699 (2021). https://doi.org/10.1109/ACCESS.2021.3069053
12. D. Kumar, O.L. Alcaraz López, S.K. Joshi, A. Tölli, Latency-aware multi-antenna SWIPT system with battery-constrained receivers. IEEE Trans. Wirel. Commun. **22**(5), 3022–3037 (2023). https://doi.org/10.1109/TWC.2022.3215864
13. A. Boaventura, A. Collado, N.B. Carvalho, A. Georgiadis, Optimum behavior: wireless power transmission system design through behavioral models and efficient synthesis techniques. IEEE Microw. Magaz. **14**(2), 26–35 (2013). https://doi.org/10.1109/MMM.2012.2234631
14. B. Clerckx, E. Bayguzina, Waveform design for wireless power transfer. IEEE Trans. Signal. Process. **64**(23), 6313–6328 (2016). https://doi.org/10.1109/TSP.2016.2601284
15. E. Boshkovska, D.W.K. Ng, N. Zlatanov, R. Schober, Practical non-linear energy harvesting model and resource allocation for SWIPT systems. IEEE Commun. Lett. **19**(12), 2082–2085 (2015). https://doi.org/10.1109/LCOMM.2015.2478460
16. E. Boshkovska, N. Zlatanov, L. Dai, D.W.K. Ng, R. Schober, Secure SWIPT Networks Based on a Non-Linear Energy Harvesting Model. In: 2017 IEEE Wireless Communications and Networking Conference Workshops (WCNCW), pp. 1–6 (2017). doi: https://doi.org/10.1109/WCNCW.2017.7919062
17. J.-M. Kang, I.-M. Kim, D.I. Kim, Mode switching for SWIPT over fading channel with nonlinear energy harvesting. IEEE Wirel. Commun. Lett. **6**(5), 678–681 (2017). https://doi.org/10.1109/LWC.2017.2729554
18. F. Wang, T. Peng, Y. Huang, Decentralized robust transceiver designs for miso swipt interference channel. IEEE Access. **6**, 4537–4546 (2018). https://doi.org/10.1109/ACCESS.2018.2791200
19. L. Jang-Won, R.R. Mazumdar, N.B. Shroff, Downlink power allocation for multi-class wireless systems. IEEE/ACM Trans. Network. **13**(4), 854–867 (2005). https://doi.org/10.1109/TNET.2005.852888
20. J. Brehmer, *Utility Maximization in Nonconvex Wireless Systems* (Springer, Berlin, 2012)
21. A. Abdel-Hadi, C. Clancy, A utility proportional fairness approach for resource allocation in 4G-LTE. In: 2014 International Conference on Computing, Networking and Communications (ICNC), pp. 1034–1040. IEEE, Honolulu, HI, USA (2014). doi: https://doi.org/10.1109/ICCNC.2014.6785480
22. J. Mo, J. Walrand, Fair end-to-end window-based congestion control. IEEE/ACM Trans. Network. **8**(5), 556–567 (2000). https://doi.org/10.1109/90.879343
23. M. Jaggi, Revisiting Frank-Wolfe: Projection-Free Sparse Convex Optimization. In: Proceedings of the 30th International Conference on International Conference on Machine Learning. ICML'13, vol. 28, pp. 427–435. JMLR.org, Atlanta, GA, USA (2013)
24. K.B. Petersen, M.S. Pedersen, *Matrix Cookbook* (Technical University of Denmark, Denmark, 2012)
25. K. Sikorski, Bisection is optimal. Numerische Mathematik **40**(1), 111–117 (1982). https://doi.org/10.1007/BF01459080
26. J. Medbo, P. Schramm, Channel models for hiperlan/2 in different indoor scenarios. Technical Report 3ERI085B, European Telecommunications Standards Institute (1998)
27. E. Boshkovska, D.W.K. Ng, N. Zlatanov, A. Koelpin, R. Schober, Robust resource allocation for MIMO wireless powered communication networks based on a non-linear EH model. IEEE Trans. Commun. **65**(5), 1984–1999 (2017). https://doi.org/10.1109/TCOMM.2017.2664860
28. K. Ntougias, I. Krikidis, G.K. Papageorgiou, M. Sellathurai, Hybrid Precoding for MISO Broadcasting SWIPT Systems: A Stochastic Optimization Approach. In: 2020 IEEE 31st Annual International Symposium on Personal, Indoor and Mobile Radio Communications, pp. 1–7 (2020). https://doi.org/10.1109/PIMRC48278.2020.9217241
29. Y.T. Chang, S. Claessens, S. Pollin, D. Schreurs: A Wideband Efficient Rectifier Design for SWIPT. In: 2019 IEEE Wireless Power Transfer Conference (WPTC), London, UK, 2019, pp. 26-29, https://doi.org/10.1109/WPTC45513.2019.9055666
30. Y. Liang, Y. He, J., Qiao, A. P. Hu: Simultaneous Wireless Information and Power Transfer in 5G Mobile Networks: A Survey. In: 2019 Computing, Communications and IoT Applications (ComComAp), , Shenzhen, China, 2019, pp. 460-465. https://doi.org/10.1109/ComComAp46287.2019.9018837
31. Inc. (2018a), M.: Filter Input Signal through MIMO Multipath Fading Channel - MATLAB - MathWorks Benelux. https://nl.mathworks.com/help/comm/ref/comm.mimochannel-system-object.html (2018)

32. R.K. Jain, D.-M.W. Chiu, W. R. Hawe: A Quantitative Measure of Fairness and Discrimination for Resource Allocation in Shared Computer Systems. Technical report, Eastern Research Laboratory, Digital Equipment Corporation, Hudson, MA (September 1984)

## Publisher's Note

Springer Nature remains neutral with regard to jurisdictional claims in published maps and institutional affiliations.